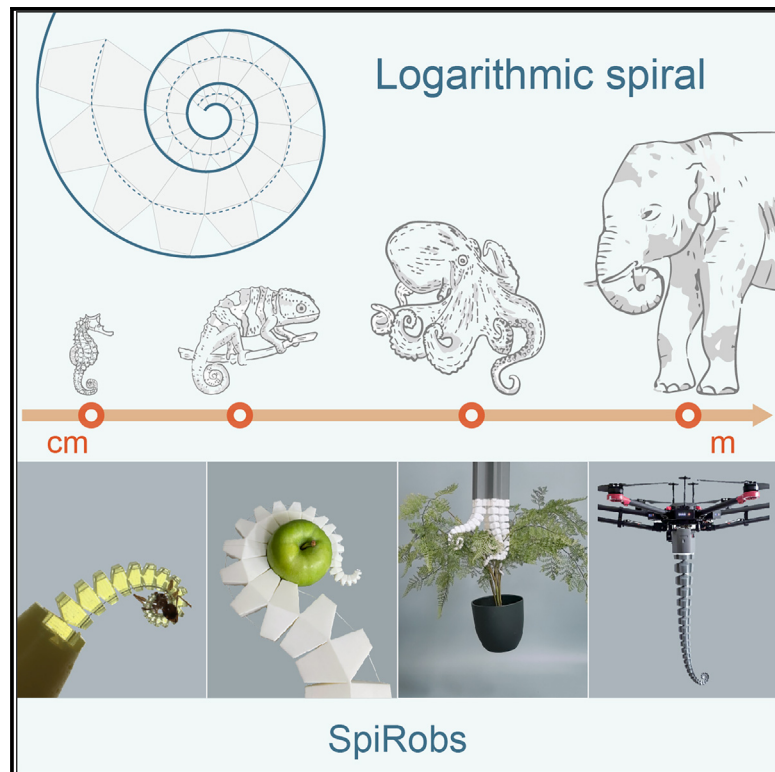


SpiRobs: Logarithmic spiral-shaped robots for versatile grasping across scales

Graphical abstract



Highlights

- A bioinspired universal design principle based on the logarithmic spiral
- Fast and low-cost fabrication based on 3D printing with TPU
- A simple actuation mechanism by two or three cables
- Numerous prototypes (ranging in length from centimeters to meters) and multi-robot arrays

Authors

Zhanchi Wang, Nikolaos M. Freris, Xi Wei

Correspondence

nfr@ustc.edu.cn (N.M.F.),
wx@ustc.edu.cn (X.W.)

In brief

SpiRobs morphologically replicate the logarithmic spiral that is ubiquitous in natural organisms. They are easy and fast to build across scales via 3D printing. They are actuated by cables, which allows for fast and life-like movements. Besides, a single robot can handle a wide variety of objects (in terms of size, shape, and weight). A key to this is a bioinspired grasping strategy that is found in the octopus. Finally, this work demonstrates a wide range of prototypes, including a miniaturized gripper, a manipulator mounted on a drone, and multi-robot arrays that can grasp in a tendril-like fashion.



Develop

Prototype with demonstrated applications
in relevant environment

Wang et al., 2025, Device 3, 100646
April 18, 2025 © 2024 The Authors. Published by
Elsevier Inc.
<https://doi.org/10.1016/j.device.2024.100646>

Article

SpiRobs: Logarithmic spiral-shaped robots for versatile grasping across scales

Zhanchi Wang,¹ Nikolaos M. Freris,^{1,3,*} and Xi Wei^{2,*}

¹School of Computer Science and Technology, University of Science and Technology of China, Hefei, Anhui 230027, China

²School of Chemistry and Materials Science, University of Science and Technology of China, Hefei, Anhui 230027, China

³Lead contact

*Correspondence: nfr@ustc.edu.cn (N.M.F.), wxi@ustc.edu.cn (X.W.)

<https://doi.org/10.1016/j.device.2024.100646>

THE BIGGER PICTURE How do we design and build robots that reproduce, as much as possible, the dexterity of octopus arms with minimal effort and cost? This paper introduces a new class of soft robots that replicate a pattern observed in nature: the logarithmic spiral. The proposed design enables lifelike movements and stable grasping through simple actuation via cables. We further demonstrate formidable scalability via numerous prototypes (ranging in size from centimeters to meters) and multi-robot arrays.

SUMMARY

Despite differences in structure and living environment, several animal appendages (e.g., octopus arms, elephant trunks, etc.) follow a common pattern: the logarithmic spiral. This paper reports a new class of soft robots that morphologically replicate the spiral based on a common design principle across scales. This allows for speedy and inexpensive fabrication, while cables are used to provide a simple yet effective control mechanism. We further present a grasping strategy, inspired by the octopus, that can automatically adapt to a target object's shape. Through extensive tests, we illustrate the dexterity of SpiRobs and the ability to grasp objects that vary in size by more than two orders of magnitude and up to 260 times self-weight. Last, we demonstrate scalability via three additional variants: a miniaturized gripper, a 1-m-long manipulator mounted on a drone, and an array of SpiRobs that can tangle up various objects.

INTRODUCTION

Animals possess highly flexible appendages across different scales; for example, the prehensile tails of seahorses and chameleons, which span a few centimeters,^{1,2} up to the meter-long arms of octopuses and trunks of elephants.^{3,4} These appendages enable a wide range of movements for various purposes, including prey capture, locomotion, manipulation, and defense. Bioinspiration has been a key driving force for building soft robots.^{5–7} Nevertheless, despite the successful demonstration of designs that can handle delicate or irregular objects,⁸ are safe for human-robot interactive tasks,^{9,10} and have found medical applications,^{11,12} existing solutions still fall short of natural beings in terms of dexterity and agility. For example, an elephant's trunk can both delicately wrap a 3 cm carrot and lift 300 kg logs,¹³ while an octopus can reach and capture prey on a sub-second timescale.¹⁴

Trying to bridge this gap faces three main challenges. First, there is a requirement for high deformability. Take the octopus arm, for example; its arms are capable of virtually continuous deformation (e.g., bending by nearly 180° at any position¹⁵). A number of soft manipulator designs have been presented with

different actuation methods, including pneumatic^{16–18} and cable driven.^{19–21} However, most of these prototypes can only produce arc-shaped bends with a limited curvature at the tip: this restricts their ability to conform to a wide range of objects, especially small ones. The use of soft materials (such as silicone) can increase the bending range and improve flexibility.^{22,23} However, this may result in wrinkling and buckling under large actuation forces, which, in turn, means failure to maintain a firm grasp. In conclusion, the use of soft materials alone is insufficient: soft is needed for dexterity, but too soft will fail to bear reasonable loads.

Second, it is crucial to develop grasping strategies that exploit the robot's flexibility. To that end, it would be beneficial to leverage the passive deformation caused by interacting with objects.²⁴ There are several demonstrations of the ability of soft robots to grasp various objects without the need for complex sensing and control, either by wrapping around^{25–28} or by using soft "fingers" to envelop.^{29,30} However, these robots can typically only produce a single repetitive pattern (such as bend and release). Grissom et al. designed a multi-segmented, pneumatically actuated arm that can grasp and move objects.³¹ In conclusion, there is a lack of "universal" strategies for reaching,

grasping, and transporting objects of different shapes and from different positions (in contrast to rigid robots, albeit at the cost of high complexity for planning and control). Developing such is a crucial step toward approaching (to the extent possible) the remarkable functional versatility of octopus arms.

Third and last, it is desirable to devise solutions that are scalable (in terms of size) to diverse target applications. However, the vast majority of existing prototypes are case specific, relying on extensive simulations alongside trial and error.³²

We observed that, despite the large diversity in terms of size (e.g., from centimeters to meters), anatomy (e.g., pure muscular or synergy of skeleton and muscles), and living environment (e.g., on land or in water), several animal appendages share a commonality in the form of a tightly packed shape that conforms to a logarithmic spiral (Figures 1A and S1).^{33–35} In addition, curling/uncurling of the spiral is critical for its function; for instance, elephants curl their trunk from the tip to pick up objects on the ground, while octopuses uncurl their arms to reach targets. Therefore, this study's goal is to go beyond specific animal examples and describe the design, fabrication, and operation of a class of soft robots from a geometric standpoint (the logarithmic spiral).

We present two principles to enable the recreation of logarithmic spiral-shaped curling/uncurling in an artificial system. First, we introduce a universal (across scales) design based on discretizing and uncurling the logarithmic spiral (Figures 1 and 2). This allows effortless fabrication of diverse robots (Figure 1D). Second, we develop a grasping strategy, inspired by the octopus, that enables the spiral-shaped body to reach and wrap around objects by controlling the curling/uncurling motion using cables (Figure 3). This strategy specifically capitalizes on the passive deformation upon contact to adapt to objects of variable shapes and sizes (e.g., cup, pen, egg, strawberry, pineapple, and more; Figure S7; Video S6) as well as to operate in confined spaces (Video S7) without the need for precise feedback or complex planning and control. Besides, we demonstrate scalability via three applications: a miniaturized SpiRob for handling minuscule biological samples (e.g., an ant, as shown in Figure 4 and Video S14), a 1-m-long SpiRob attached to a drone for performing dynamic grasping tasks (Figure 5; Video S19), and an array of SpiRobs that can pick up various objects through entanglement (Figure 6; Video S20).

RESULTS

Design of SpiRobs

The logarithmic spiral (also known as growth spiral) is represented in polar coordinates (ρ, θ) by $\rho = ae^{b\theta}$, where $a > 0$ and b are scaling parameters. Our design is based on the discretization and uncurling of a logarithmic spiral via the following process (Figure 1B). We first construct what we call the central spiral, which is defined as the curve formed by the midpoints of the line segments connecting points on the spiral that differ in phase by 2π : $\rho_c(\theta) = \frac{\rho(\theta) + \rho(\theta+2\pi)}{2}$. We then consider rays from the origin corresponding to fixed angle intervals ($\Delta\theta$); connecting the points of intersection with the original and central spiral forms a series of quadrilaterals. Finally, by mirroring these with respect to the central spiral, we form the discrete units of the robot's body

(Figure 1B). Note that, once the spiral parameters (a and b) and discretization step ($\Delta\theta$) are given, the shape and size of the units are fully determined (experimental procedures; Design of SpiRobs); in fact, adjacent units are at a fixed ratio (Fabrication of SpiRobs), which allows us to simply design a single unit and just scale it up/down to obtain a SpiRob of any scale. The uncurling of these units naturally results in a tapered body. This can be curled and wrapped back under the forces acting through a cable passing through the robot's body, with one end fixed to the tip through a knot and the other connected to the motor (Figure 1C; Video S1).

An elastic layer is added on the central axis that connects discrete units; this provides the restoring force for the robot to uncurl when the cable is relaxed. Extruding the 2D design pattern generates a 3D solid entity, which we cut to obtain a hexagonal cross-section (Figure 2A). This serves to maintain tapering across all sides of the robot in 3D as well as to reduce the inertia, which, in turn, provides higher flexibility for the tip motions. Then, we punch holes of appropriate sizes for the cables to pass through in the final computer-aided design (CAD) drawing and fabricate the robot by 3D printing (Bambu Lab X1C, thermoplastic polyurethane [TPU]@95A, see Figure S2, Note S1, and supplemental experimental procedures for printing and assembly guidelines).

The units of SpiRobs decrease in size from the base to the tip (at a fixed ratio; see Jiang et al. and Equation 9). This is because the uniform discretization we apply is on the angular domain ($\Delta\theta$), which is the key for the robot to curl into a logarithmic spiral. The radius of curvature (when packed) decreases from the base to the tip (it is affine to the length from the tip of the robot to that point; see Hauser and Hughes, Equation 7, and Table S1). This indicates higher flexibility close to the tip and is instrumental for the potency of SpiRobs when wrapping and grasping a wide range of objects (especially small ones). It constitutes a critical difference from existing designs, which mostly deform in a constant-curvature manner.³⁶ To visualize this, we plot the graspable space (defined as the set of positions where the smallest graspable object can be grasped) in Figure 2B. The comparison with two alternative designs corroborates the advantages of our design (Figure S3).

The thickness of the elastic layer ($\sigma(\theta)$ in Figure 2A) influences the movement of the robot. We designed prototypes with elastic layer thickness ranging from 2.5% to 12.5% in 2.5% increments (the percentage denotes the ratio $\sigma(\theta)/\delta(\theta)$). A thinner elastic layer is likely to cause collisions with the base (Figure 2C, cases ① and ②), while a thicker layer requires a larger force to bend (Figure S3C; Video S2). To trade off between force and curling success rate, we selected a value of 5% for the thickness of the elastic layer in 2-cable SpiRobs.

Selecting the taper angle constitutes another crucial design choice. We designed three SpiRobs with different taper angles (5°, 10°, and 15°) but common lengths and tip diameters (Figure 2D). We found that the envelope of the workspace also admits a spiral shape (Figures 2E and S4; Note S2). Furthermore, the simulation in MuJoCo³⁷ validates that all interior points are reachable (Figures 2E and S5; Note S3). In addition, we can analytically characterize the relationship between the size and weight of objects that can be grasped (Note S2). The following

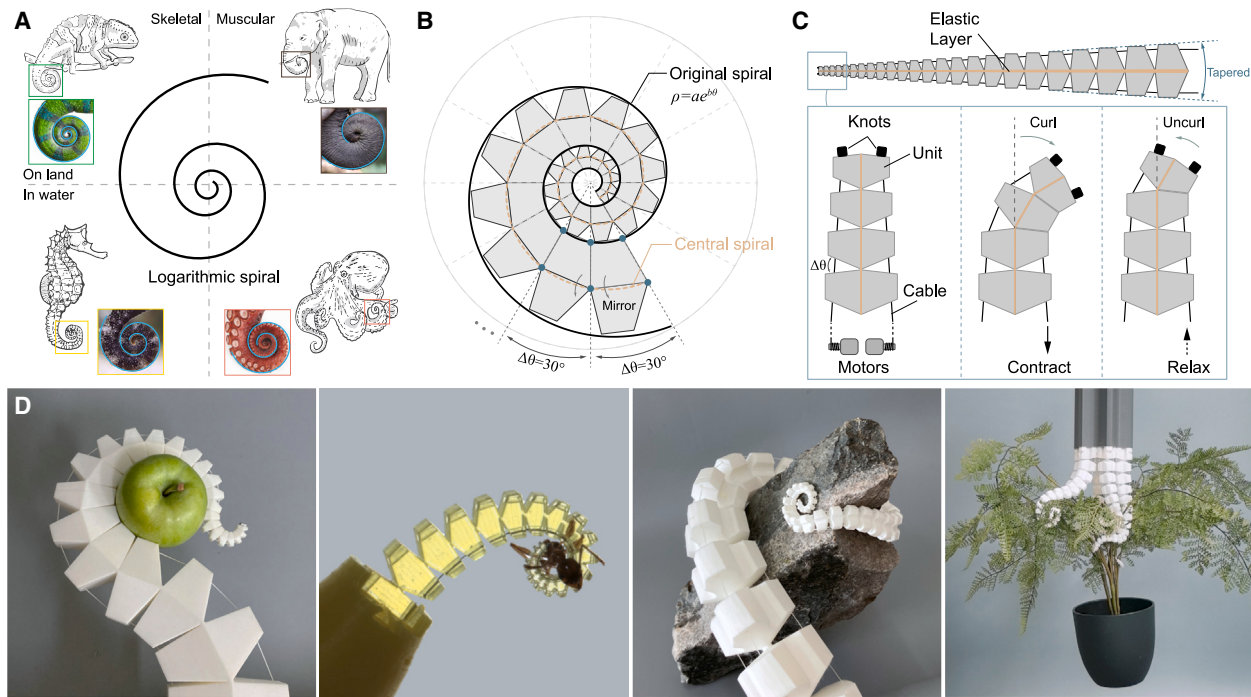


Figure 1. Bioinspiration and design principle of spiral robots

- (A) Examples of animal parts that follow the logarithmic spiral. We provide the fitted spirals with blue lines.
- (B) Design of SpiRob. The logarithmic spiral ($\rho = ae^{b\theta}$) is discretized with a fixed step ($\Delta\theta$), and the resulting quadrilaterals are mirrored over the central spiral to obtain the robot units.
- (C) An elastic layer is added on the central axis. The contour of the robot body (top, dashed lines) forms a cone with a fixed taper angle. The cables are connected to motors and attached to the tipmost unit by knots. The cable contraction and relaxation are translated into the robot curling and uncurling.
- (D) Images of multiple SpiRobs: a 2-cable robot holding an apple, a miniaturized robot grasping an ant, a 3-cable robot wrapping around a rock, and an array of SpiRobs tangling up a plant. All robots were fabricated by 3D printing.

conclusions are drawn for fixed length and tip diameter. The smaller the taper angle, the larger the workspace (Figure 2E). At the same time, the larger the taper angle, the smaller the diameter of the smallest object that can be grasped and the larger the maximum load capacity; besides, for fixed diameter, the larger the weight (with the difference more pronounced for large-sized objects; Figure 2F and Note S2). Taking the robot with a taper angle of 15° as an example, it can grasp objects whose diameters vary by two orders of magnitude (from 5.6 to 115 mm) and weigh roughly 260 times the weight of the robot (38.4 g self-weight and 10 kg load capacity; see Figure 2G and Note S2 for the theoretical justification).

Bioinspired grasping strategy

Our strategy enables reaching, wrapping, grasping, and transporting different objects by controlling the robot's curling/uncurling motion. This movement pattern is reported in the octopus^{3,38}: it progressively uncurls and straightens curled arms to reach the target. After making contact with the object, the arm keeps uncurling on the surface of the object to align the suckers (Figure 3A; Video S3). For a 2-cable SpiRob, this is accomplished by controlling the cable forces: when only the left or right cable is stretched, the robot curls to the left/right to tightly pack into a spiral. By jointly controlling the forces exerted to the two cables (in an antagonistic manner), the robot reaches out, contacts the

object, and uncurls the body along the object's surface to wrap around and grasp it (Figure 3A; Videos S3 and S6). We call the uncurling movement on the object's surface "climbing," similar to a plant (e.g., ivy) climbing on the wall. Similar grasping strategies are reported for multi-joint rigid robots³⁹; however, our design allows for a far simpler implementation without the need for a deliberately designed pulley series.

We verified the effectiveness of this grasping and manipulation principle on a real robot (24 units for a total length of 45 cm; Figures 3B, S6, and S7; Notes S4 and S5) and in simulations (where we use a model based on serial elastic joints; Video S8). Unlike fingertip-based grasping,⁴⁰ the proposed strategy exploits the entirety of the robot's body to contact and wrap around the object. This is advantageous because a larger contact area means greater load capacity and grasping stability. We want to highlight that, although our design does not include suckers like the octopus, uncurling the packed body on the surface of an object suffices for wrapping and grasping. Besides, during climbing, the robot's body does not slide relative to the contact surface, which is key for automatically adapting to objects of different shape and roughness. At the same time, this also enables the robot to easily navigate through confined spaces (the last two rows in Figures 3B and S8; Video S7). We further conducted a quantitative experiment to evaluate the graspable space of the proposed strategy for objects of

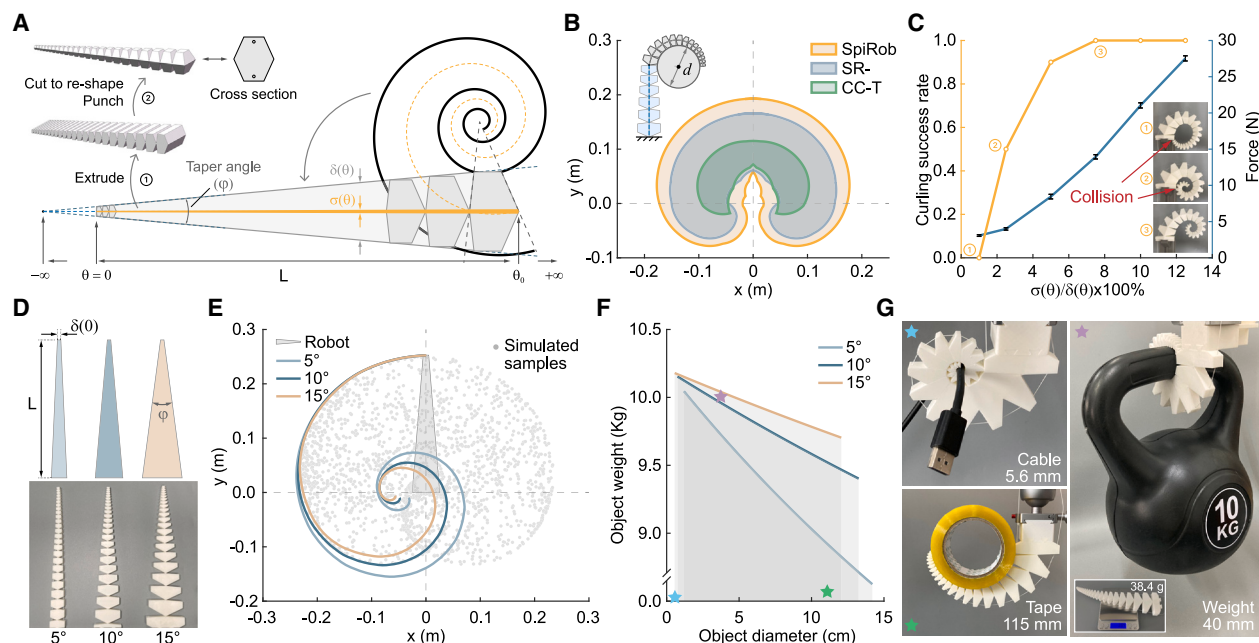


Figure 2. Design parameters

- (A) A computer-aided design (CAD) model of a 25-cm-long SpiRob driven by two cables. First, the 2D discretized pattern is extruded to obtain a 3D solid (step ①), which is then cut into a conical shape, and two holes are reserved for the cables to pass through (step ②).
 (B) Comparison of the workspaces of different designs when holding the smallest graspable object: SR-, a SpiRob with lower deformation capability (obtained by decreasing the gaps while keeping the unit lengths fixed); CC-T, a tapered constant-curvature robot.
 (C) Effect of elastic layer thickness on curling. If a thin layer is used, then the robot will collide with the base. Increasing the thickness can solve this problem, but it also means that a greater force is required to curl the robot into a spiral.
 (D) SpiRobs with different taper angles: 5°, 10°, and 15°; L is the length of the robot, and $\delta(0)$ is the width of its tip ($L = 25$ cm and $\delta(0) = 5.5$ mm in this case).
 (E) Workspace: the smaller the taper angle, the larger the workspace. The workspace envelopes are calculated as in Note S2. The gray dots illustrate the reachable points (10° robot) generated by randomly sampling cable forces in simulation based on a joint-link model (Note S3).
 (F) Theoretical predictions (Note S2) of the object size and weight that can be grasped with a maximum actuation force of 100 N: a larger taper angle means a larger weight for a fixed diameter.
 (G) Images of a SpiRob (15°) grasping a 5.6-mm-diameter cable, a 115-mm-diameter tape, and a 10 kg weight. Stars in (F) and (G) are used to match the experiments to the weight-diameter plot.

different sizes. We divided the right half of the workspace into a grid of 5×5 cm cells, selected three objects of different diameters (25, 50, and 100 mm), and carried out grasping tests at each grid point (Figure 3C). We found that the smaller the diameter, the closer the farthest point that can be grasped is to the boundary of the workspace. In particular, the same object may not be graspable if placed too far or close.

To automate the grasping, we propose a method to detect contact with an object as well as a simple rule (piece-wise linear actuation; Figure 3A) to control the cable forces by relating them directly to the object's position. Regarding the former, we noticed that there is an increase in the current drawn by the motor when the robot contacts an object (because the motor tries to maintain a constant speed of motion). This can be leveraged for contact perception. The threshold for detection was set through multiple experiments, and this simple mechanism was shown to be capable of detecting even the slightest contact; e.g., with a feather (Figure 3D; Video S4). Regarding the latter, we first note that the force on the left cable at the beginning of the reaching stage (F_1^0) represents how tightly the robot is packed. This affects how easily the robot can uncurl when the right cable is pulled, which,

in turn, determines the trajectory followed by the SpiRob when reaching out. Based on this observation, we adopt a simple universal rule to define F_1^0 as a function of the target object's position (p, α) in polar coordinates. Namely, we consider a linear relationship $F_1^0 = -c_1 p + c_2 \alpha + c_0$, where $c_{0,1,2} > 0$ are constants (determined experimentally as $c_0 = 14$, $c_1 = 13$, and $c_2 = 5$). The intuition behind this choice is as follows: a smaller force allows the robot to reach farther (hence the use of $-c_1 < 0$). Besides, the larger the yaw angle of the object, the greater the force needs to be to avoid premature uncurling. This method only requires the object's approximate location (e.g., as obtained by a camera; Kinect V2, Windows), circumventing the need for high-frequency feedback or precise motion planning. Together with the contact detection mechanism, we managed a consistently high success rate in grasping objects of different shapes (~95% success in the experiments in Figure 3E; Video S5).

Scalability

Small-scale SpiRobs

We scaled down the 2-cable robot shown in Figure 3 by 70 times to a length of about 1 cm across 29 units with a tip diameter of

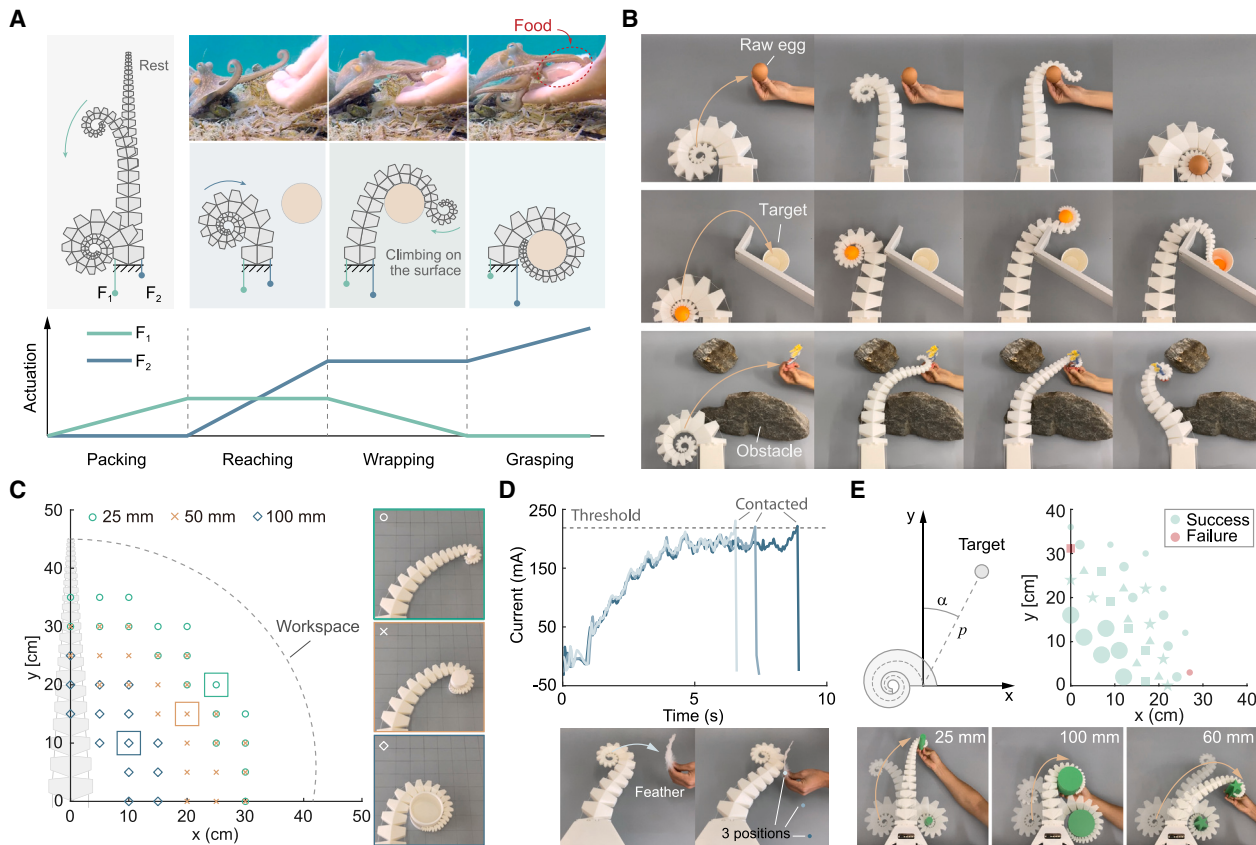


Figure 3. Grasping

(A) Snapshots of an octopus progressively uncurling its arm to reach, wrap, and grasp food (original video credits: <https://www.youtube.com/watch?v=GdCOYToDqfM>). Inspired by this, we developed a strategy to replicate this motion by controlling the forces on two cables. Starting from a resting state (no force), we increase the force on the left cable, causing the robot to curl into a spiral from the tip (packing). Next, we increase the force on the right cable (F_2) while keeping the one on the left (F_1) unchanged, allowing the robot to uncurl from the base and reach out toward the object (reaching). Once in contact with the object, we slowly reduce the force on the left cable while maintaining the one on the right, enabling the robot to climb up the object's surface and wrap around it (wrapping). Finally, we increase the force on the right cable to secure a firm grasp (grasping).

(B) SpiRobs grasping and moving various objects: grasping a raw egg, transporting a ping pong ball to a target behind the wall, and reaching through a crevice to grasp and retrieve a target object (more tests are shown in Figures S7 and S8).

(C) Graspable space for different-sized objects with the proposed strategy. Colored points represent the locations where objects (represented by different markers) can be grasped successfully. The envelope of the workspace is plotted as a dashed gray line.

(D) The robot senses the contact with a feather by detecting changes in the current. By repeating this across three trials (different positions), we determine that the same threshold can be used for contact detection across the workspace while maintaining high sensitivity. This detection mechanism can be used to initiate the reaching and wrapping stages of our strategy.

(E) The robot automatically grasps objects of different geometries with the minimal information of object positions (p, α) obtained by a camera. Objects of different sizes are placed within the approximate area identified in (C).

0.14 mm (Figure 4A). We use a resin (ST1400, BMF) to fabricate the robot through stereolithography 3D printing (Microarch S130, BMF). Two cables that are 20 μm in diameter pass through the robot's body and bond with the resin at the tip (Figure 4C). They are controlled by two sliders on a pen-shaped handle (Figure 4B). We demonstrate that this design can handle an ant without breaking it (Figure 4D; Video S14).

Three-cable SpiRobs

We also fabricated a 1-m-long robot (42 units with a tip/base diameter of 5 mm/12 cm; see [supplemental experimental procedures](#) for a step-by-step build guide) that is actuated by three cables spaced evenly across the circle engulfing the cross-sec-

tion (Figure 5A). We first obtain a series of parts by discretizing the spiral (as in Figure 1) and then generate a 3D entity by rotation (in place of the mirroring used for 2-cable robots). An elastic axis (10% thickness) connects the discrete units. We further cut to reshape the cross-section (Figure 5A) for two purposes: (1) to reduce the overall inertia and (2) to increase the contact area when the robot grasps the object. The length of this robot exceeded the working area of the 3D printer, so we printed it in four segments and assembled them using dovetail connectors (Figure 5E).

We manually operate the three cables with a strategy similar to the one described previously: the robot unfolds its curled body

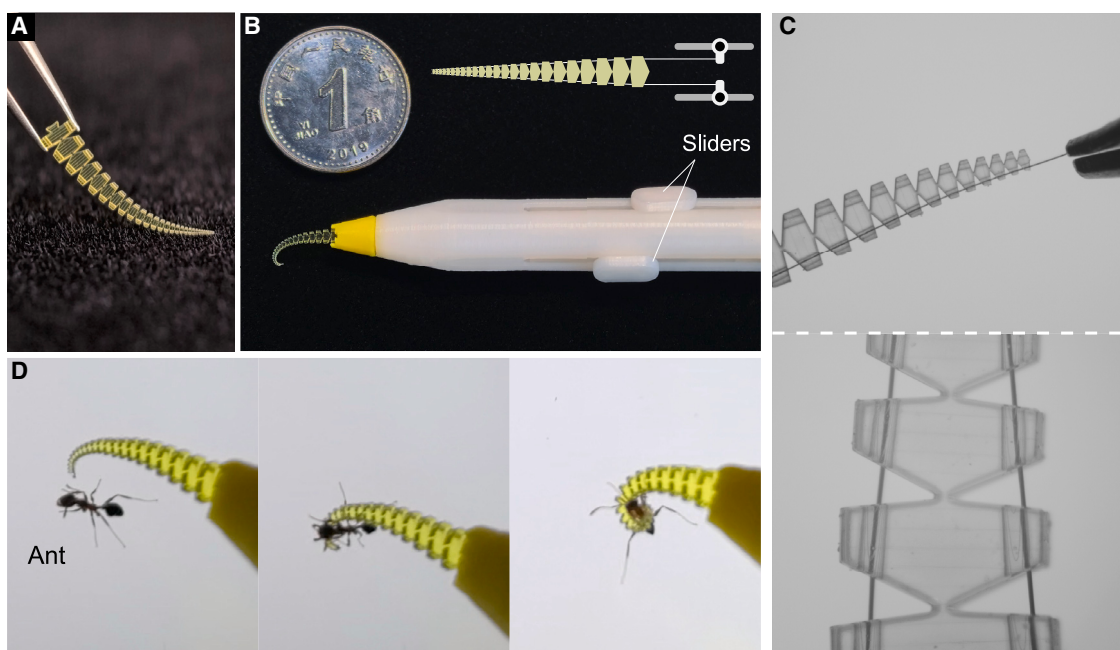


Figure 4. SpiRob for non-invasive grasping of small living organisms

- (A) A 3D printed miniaturized (millimeter-scale) SpiRob.
(B) System assembly. The two cables are connected to two sliders, and the robot can be curled in two directions by moving the sliders.
(C) Photographs of the cables and the robot.
(D) Delicate grasping of an ant with the miniaturized SpiRob.

on the object's surface to wrap around and grasp it (Figures 5B and S14; Videos S15 and S16). For dynamic operations in 3D space, higher flexibility can be achieved due to the intrinsic inertia and stiffness of the body and the effect of gravity. With a simple sawtooth actuation to one of the cables, the robot's body will curl up and reach a specific position, after which uncurling yields a whipping motion (Figures 5C and S13; Video S17). Besides, an additional "curling" command (pulling the other two cables) can be used to grasp, as illustrated by grasping and lifting a headset within 1 s (Figure 5D; Video S18).

Additionally, we attached the robot and its control terminal with three motors (Figure S2C; Note S6) to a drone and conducted a grasping test by remote control (Figure 5B). The drone was controlled to hover near a bucket (with a 1 kg load inside), and the SpiRob was commanded to whip toward the bucket handle to grasp it (Figure 5F; Video S19; visual feedback by an onboard camera was used).

Multi-SpiRob array

We also built a gripper comprising multiple SpiRobs (each 3 cable and 25 cm in length with a tip/base diameter of 5/30 mm) evenly arranged on the circumference of a circle (Figure 6A). We attach this to a rigid arm (Figure 6B) to perform grasping by entanglement; our design was shown to be effective for 10 objects that are entirely different in terms of size and shape without the need for any perception or feedback control (Video S20). We also evaluated the effect of the number of arms on the success of grasping (Figure 6C); for an array of six SpiRobs, the gripper can achieve a success rate of more than 90%. Increasing the number of arms does not significantly

improve the success rate (because a circle of a larger diameter is needed to distribute the arms, so that grasping a smaller object, like a tennis ball, is more likely to fail). We also measured the load capacity (defined as the force required to pull an object out of grasp) using a force sensor. We 3D printed five tree-shaped targets with different numbers of branches (2, 4, 8, and 16, as shown in Figure 6D). We found that the more complex the shape of the object, the more secure the grasp due to a higher level of intertwining. We would like to point out that a similar concept was introduced by Becker et al.⁴¹ Further visualization can be found in Figure 6E and Video S20.

DISCUSSION

The design principle based on the logarithmic spiral constitutes the main novelty in this study. Unlike in soft robotics, where the hardware is designed first, and the models are developed afterward, in our system, modeling (logarithmic spiral) comes first, and design/fabrication is a direct outcome of the model. This allows designing SpiRobs for a large diversity of application scenarios (i.e., in terms of grasping size and load capacity; Table S1) instead of using a trial-and-error approach and resorting to extensive simulations.

The spiral has been exploited in various robot designs. Zhang et al. and Zournatzi et al. built spiral-shaped molds to fabricate pneumatically actuated soft robots that unfold when pressurized.^{30,42} However, the constant-width cross-section prohibits spiral deformation (Figures S15A and S15B). Taylor et al. devised a cable-driven serpentine-like structure,²⁸ while Wang et al.

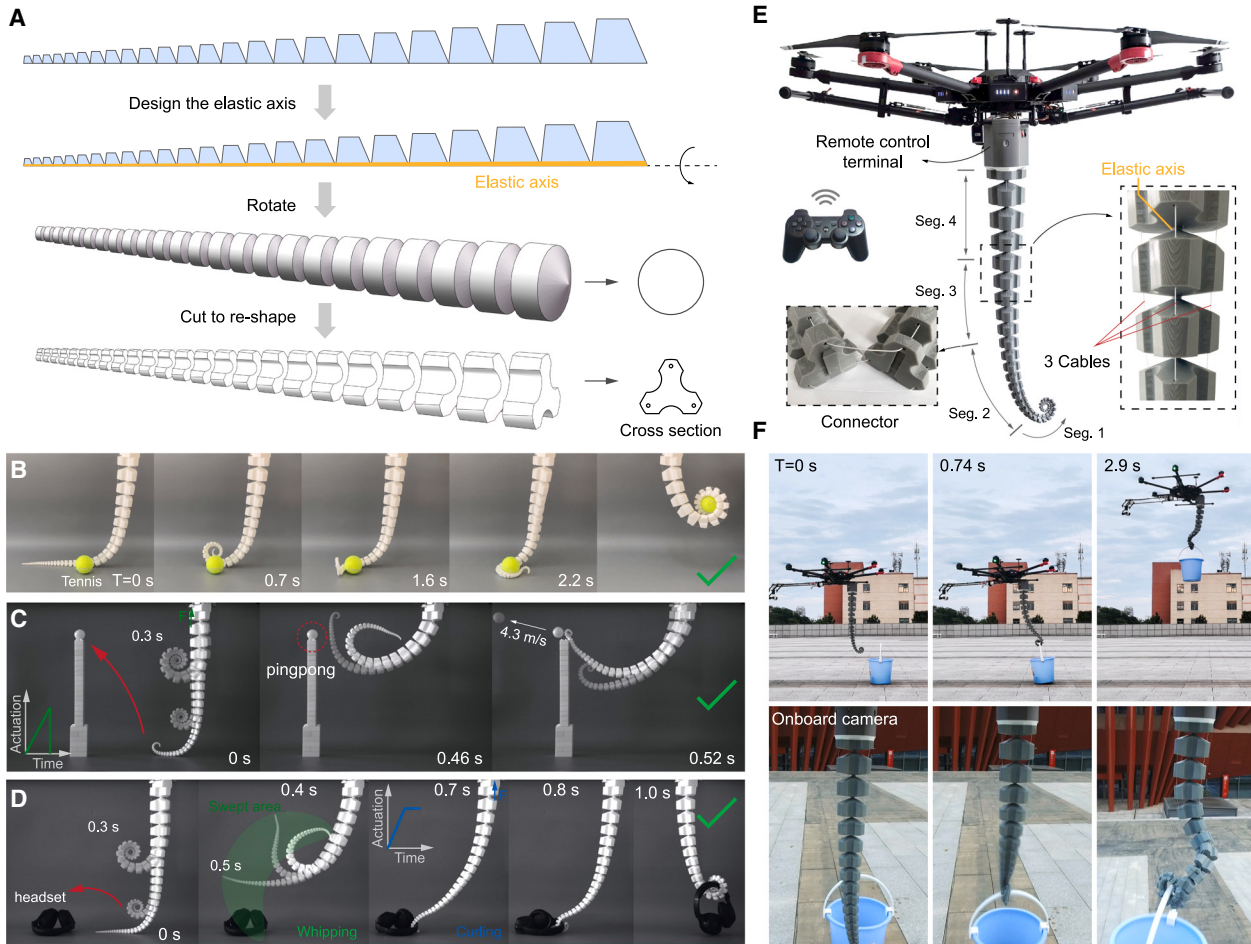


Figure 5. Large-scale 3-cable SpiRobs

- (A) Design of a 3D deformable SpiRob. We first rotate the parts around the central axis to form a cone-shaped body, which we then cut to obtain a cross-section that increases the contact area when wrapping around objects (while also reducing the total inertia).
- (B) Image sequence of a SpiRob picking up a ball from the table; the length of the robot is 1 m, and it comprises four parts assembled using dovetail connectors with a cylindric central axis serving as the elastic layer (see E).
- (C) Whipping. The robot dynamically reaches a point on a sub-second timescale to bounce a ping pong ball with a simple sawtooth actuation.
- (D) The robot grasps and lifts a headset within 1 s.
- (E) Mounting on a drone.
- (F) Image sequence of grasping a bucket; both the robot and drone are operated by remote control.

manufactured a thermally driven tendril-like gripper.⁴³ Both of these can achieve spiral deformations to some extent (see Figures S15E and S15G, the former via variable stiffness across the body and the latter due to different elongation rates of the two materials comprising its body). Nonetheless, spiraling can only follow a single repetitive pattern determined by the fabrication process. This is in sharp contrast with SpiRobs, where spiraling can happen at any point of the body in a controlled manner (a key attribute for versatile manipulation). Even rigid robots have leveraged the spiral. Edmark used laser-cut plywood to fabricate a multi-segmented robot that can curl into a spiral when pulling a cable⁴⁴ (Figure S15I). Sugiura et al. built a robot that can unfold from a spiral shape to a straight shape to support individuals with mobility impairments⁴⁵ (Figure S15J). Nonetheless, in both cases, spiraling was pre-determined, while there

was also no demonstration of object grasping. The unique contribution of the present study is that it is the first (to our best knowledge) to introduce a design that replicates the logarithmic spiral not just in shape but in deformations at each point of the body. The end outcome is fast fabrication (using inexpensive 3D printing) of robots that feature life-like speed and versatility, albeit with a very simple actuation mechanism.

The bioinspired grasping strategy achieves high adaptability and grasping stability. For instance, it greatly increases the grasping space compared to direct bending (Figure S6). However, it is worth noting that, when the SpiRob climbs on the surface of an object, it exerts a force that may push it away (we measure this in Figure S9). Still, we have noticed this not to be a severe issue; e.g., when grasping a strawberry that is not fixed (Figure S7) or a ball placed on a table without bumping it away

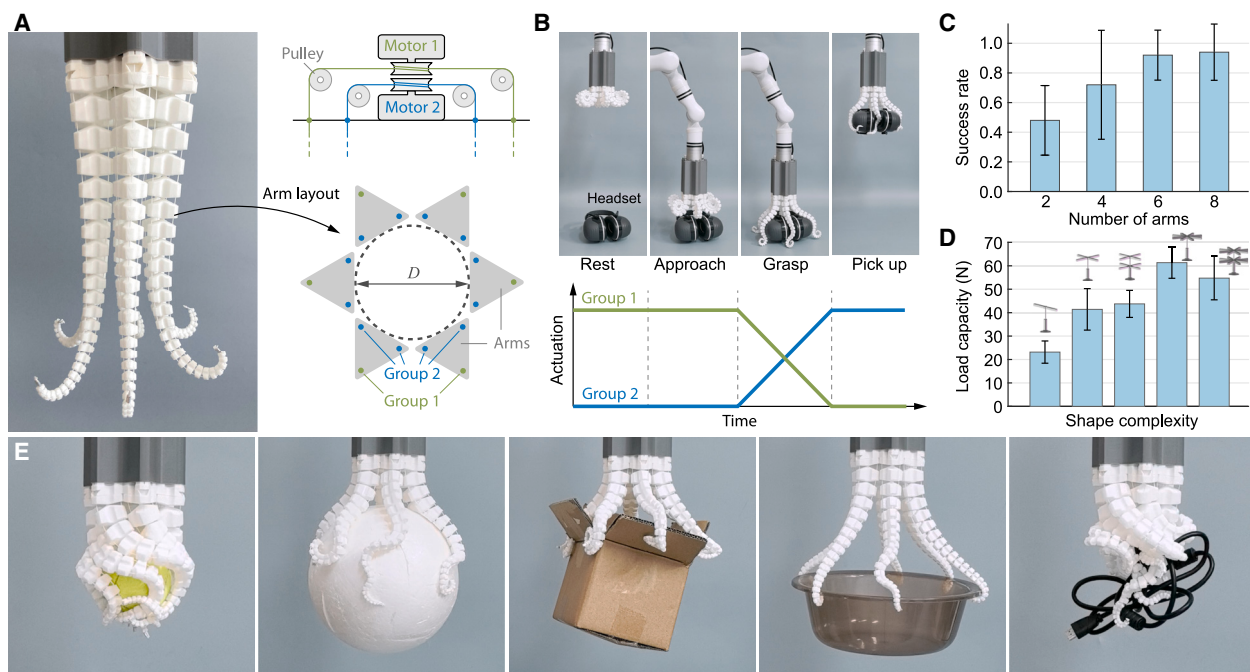


Figure 6. An array of SpiRobs used as a gripper

- (A) A multi-arm gripper consisting of 6 SpiRob arms. Right: the layout of the arms and how they are driven. The cables are divided into two groups: outer (group 1) and inner (group 2), each controlled by a (common) motor. Pulling the outer cables causes all arms to curl up, while pulling the inner cables causes them to uncurl.
- (B) The sequence of grasping with the array attached to a rigid robotic arm. The actuation patterns of the cables at different stages are plotted below.
- (C) The success rate of grasping with different numbers of arms. Ten objects of different sizes and shapes were used for testing, five of which are shown in (E) (see Table S2 for more details).
- (D) The load capacity of the 6-arm gripper was measured in a test performed with various tree-shaped objects with increasing shape complexity (i.e., an increasing number of branches).
- (E) Photographs of an array of 6 SpiRobs actuated by a maximum force of 60 N to entangle various objects.

(Figure 5B). The multi-SpiRob gripper has no such issue, since grasping is achieved by enveloping the object. Besides, the speed of the robot also plays a positive role; by quickly moving the cables, the robot can remove a tissue from a plastic box without displacing it (Figure S7G). Last but not least, we also show how the robot's tip can be guided to a target position and orientation with a similar operation strategy (Figure S10; Video S9).

A similar strategy of unfolding the robot on the object to grasp it has been shown with rigid robots. Hirose and Umetani demonstrated a robot comprising multiple serial joints (similar to a bicycle chain) that is capable of uncurling from a packed state to wrap around an object³⁹ (Figure S15K). However, under-actuation using cables fails to achieve a firm grasp. To address this, Glick et al. added adhesive parts across the body, albeit at the cost of limiting flexibility (for example, the robot body cannot touch itself; Figure S15L). In this study, we successfully implement the grasping strategy through a simple piece-wise linear control sequence of the forces on the two cables. A theoretical justification for this choice can be found in our previous work.⁴⁷

We conclude by stating the main limitation of the current status of this work, which is the absence of an inverse kinematic and dynamical model that would serve to infer the optimal cable actuation to reach a target configuration while also incorporating

feedback. This is essential for developing more general-purpose controllers than the one presented for implementing our bio-inspired grasping strategy with minimal feedback (contact detection). As a consequence, developing such models and controllers constitutes the top priority of our future work.

Conclusion

SpiRobs are bioinspired in both morphology and operation. A notable attribute is the scalability of the design principle (demonstrated with robots from centimeter to meter scale). They are capable of complex movements and feature formidable adaptability in handling objects that vary in size and shape with minimal actuation (2–3 cables). We further demonstrated three applications: (1) a miniaturized robot that can handle fragile samples, (2) teleoperation on a portable platform (drone), and (3) a multi-arm gripper that functions via entanglement.

EXPERIMENTAL PROCEDURES

Design of SpiRobs

A SpiRob consists of three main components: the robot body, the cables, and the motors. The two ends of each cable are connected to the tipmost unit and the motor, and the cable's contract/relax actuation is translated to the curling/uncurling motion of the robot, respectively. In the following, we describe the design process and determine the key parameters of the robot body.

We take a SpiRob with two cables as an example; it can wrap in two directions on a plane. Recall the expression of the logarithmic spiral ((ρ, θ) are polar coordinates):

$$\rho(\theta) = ae^{b\theta}, b = \cot \psi \quad (\text{Equation 1})$$

where $a > 0$ is a scaling factor, and b is the cotangent of the constant polar tangential angle ψ , defined as the angle between the tangent of a point on the spiral and the line connecting the point to the origin. (1) can be re-written as $\rho(\theta) = e^{b(\theta+\frac{\ln a}{b})}$, so that a can be interpreted as translation in the angular domain and b as scaling. For design, we restrict attention to the range $\theta \geq 0$. The tip corresponds to $\theta = 0$, while the range $\theta < 0$ corresponds to the extension from the tip to the point where the outer edges of the robot meet ($\theta \rightarrow -\infty$; [Figure 2A](#)). We define the “central” spiral, which characterizes the central axis of the robot ([Figure 1B](#)), by:

$$\rho_c(\theta) = \frac{1}{2}(ae^{b(\theta+2\pi)} + ae^{b\theta}) = \frac{a}{2}(e^{2\pi b} + 1)e^{b\theta} \quad (\text{Equation 2})$$

The rays starting from the origin and at fixed angle intervals ($\Delta\theta = 30^\circ$) are chosen by default for our robots unless explicitly stated otherwise) intersect with points on the original spiral and the central spiral, connecting these form quadrilaterals. This process builds one part of the robot, to which we attach an elastic layer that provides the restoring force, which is crucial for the robot’s flexibility. The other part is obtained by mirroring with respect to the central axis. In our design, the elastic layer’s thickness is chosen as 5% of the unit width for the 2-cable robots and 10% for the 3-cable robots.

The taper angle (ϕ) of the robot is related to the spiral parameters as follows:

$$\phi = 2 \arctan \left(\frac{\frac{1}{2}\delta(\theta)}{L(-\infty, \theta)} \right) = 2 \arctan \left(\frac{b(e^{2\pi b} - 1)}{\sqrt{b^2 + 1}(e^{2\pi b} + 1)} \right) \quad (\text{Equation 3})$$

where $\delta(\theta) = ae^{b(\theta+2\pi)} - ae^{b\theta}$ is the width of the robot at angle θ and

$$L(-\infty, \theta) = \int_{-\infty}^{\theta} \sqrt{\rho_c^2 + \dot{\rho}_c^2} d\theta = \frac{\rho_c(\theta)}{\cos \psi} \quad (\text{Equation 4})$$

captures the length of the central spiral from the “virtual” tip ($\theta \rightarrow -\infty$) to a given point (angle θ) ([Figure 2A](#)). The fact that ϕ in (3) is independent of θ shows that the spiral is tapered when expanded.

The length of the central axis of the robot has the following relationship with the spiral parameters:

$$L(0, \theta_0) = \int_0^{\theta_0} \sqrt{\rho_c^2 + \dot{\rho}_c^2} d\theta = \frac{\rho_c(\theta_0) - \rho_c(0)}{\cos \psi} = \frac{\sqrt{b^2 + 1}a_1}{b}(e^{b\theta_0} - 1) \quad (\text{Equation 5})$$

The lower bound in the integral here ($\theta = 0$) corresponds to the robot’s tip and the upper bound (θ_0) to the root ([Figure 2A](#)). The curvature of the robot $\kappa(\theta)$ (when packed into a logarithmic spiral) can be calculated from the expression of the central spiral to be

$$\kappa(\theta) = \frac{\sin \psi}{\rho_c(\theta)} = \frac{2}{a(e^{2\pi b} + 1)\sqrt{b^2 + 1}} e^{-b\theta} \quad (\text{Equation 6})$$

In particular, the curvature changes exponentially with θ . We further express the radius of curvature as a function of the distance of each point from the virtual tip (we denote $s \equiv L(-\infty, \theta)$ in the following). By use of (4), (6), and (1), we obtain

$$r(s) = \frac{1}{\kappa(s)} = bs \quad (\text{Equation 7})$$

This shows that the radius of curvature of the central axis changes linearly with the distance from the (virtual) tip. Moreover, the deformation ratio (γ), defined as the ratio of the lengths of the robot’s surfaces when the robot shifts

from the packing state to the left to the packing state to the right (and vice versa), can be calculated as

$$\gamma = \frac{\int_{2\pi}^{\theta+2\pi} \sqrt{\rho^2 + \dot{\rho}^2} d\theta}{\int_0^{\theta} \sqrt{\rho^2 + \dot{\rho}^2} d\theta} = e^{2\pi b} \quad (\text{Equation 8})$$

The deformation ratio is the same for all points across the robot body (parameterized by angles θ), which means that any part of the robot deforms at the same ratio. To illustrate, when $b = 0.22$ (i.e., taper angle $\phi = 15^\circ$), $\gamma = 3.98$. This is quite large for a continuous homogeneous body to undergo without deteriorating over time or even breaking from repeated stretching/shortening. Our multi-unit design (based on discretizing the spiral) is key for resolving this. This phenomenon also justifies the wrinkles and folds on the elephant trunk’s surface, providing feasibility and sustainability for large deformations.⁴⁸

Fabrication of SpiRobs

The robots are built using a desktop 3D printer (X1CC, Bambu Lab) with a 1.75 mm TPU filament (eTPU-95A, eSUN; [Figure S2A](#)). Note that adjacent units of the robot are at a fixed ratio

$$\beta = \frac{\delta(\theta + \Delta\theta)}{\delta(\theta)} = e^{b\Delta\theta} \quad (\text{Equation 9})$$

where $\Delta\theta$ is the discretization step. Thus, we only need to design one unit and then scale up/down according to the factor β to obtain the adjacent ones. Second, longer robots can be fabricated in segments connected by a dovetail connector ([Figure S2A](#)). The 2-cable robot in [Figure 3](#) consists of two segments, and the 3-cable robot in [Figure 5](#) consists of four segments. We designed small holes on each unit for the cable to pass through. We use ultra-high-molecular-weight polyethylene cables for the robot’s actuation. This cable type is wear resistant and smooth, thus reducing friction as it moves through the robot’s body. Furthermore, the cable is fastened to the tip unit with a fisherman’s knot to ensure that the actuation force is transmitted without slipping.

SpiRobs conducting dynamic tasks

We illustrate that SpiRobs portray favorable capabilities analogous to living organisms: high-speed dynamic movement and impact resistance with robust grasping. On a sub-second or second timescale, octopuses can grab and catch a fish, while elephants can use their trunks to spray water all over their bodies. Here, we demonstrate similar attributes through simple open-loop or manual control ([Video S10](#)). Grasping was achieved in as little as 60 ms ([Figure S11A](#); [Video S1](#)). Besides, passive deformation allowed catching objects of different sizes moving at high speed ([Figure S11B](#); [Video S11](#)). Moreover, the robot was shown to feature formidable grasping stability that can resist out-of-plane torsion and dynamic impact ([Figure S11C](#); [Video S12](#)).

Additionally, we conducted several instances of “elephant throw” and “whipping.” For the former, high-speed uncurling can throw objects at 10.5 m/s ([Figure S12](#); [Video S13](#)). For the latter, the intrinsic stiffness of the body and the effect of gravity are exploited; the curled body “shoots” out to reach a specific position ([Figures 5C and S13](#); [Video S17](#)) or grasp objects ([Figure 5D](#); [Video S18](#)). By throwing objects in different directions and whipping at different positions, we demonstrate the repeatability and controllability of the motion of the SpiRobs.

Control terminals

We built three motor control terminals used to drive different robots. First, the terminal for the 2-cable robot operations consists of two motors (GM6020, DJI; [Figure S2B](#)), an embedded controller (Robomaster Development Board, type A, DJI), and a 24 V battery. The motors are direct-drive brushless without a gearbox and can be controlled for torque, speed, and position. This also provides the basis for our current-based contact detection. Second, the terminal for the 3-cable SpiRob (in the drone application; [Figure S2C](#)) consists of three motors (M2006, DJI) and an embedded controller (Robomaster Development Board, type C, DJI). The terminal has a 2.4 GHz wireless communication

module that connects to the joystick for remote control. The drone supplies the power to reduce the weight of the system. Finally, the terminal for the multi-SpiRob grippers consists of two motors (M2006, DJI; **Figure 6B**), a microcontroller (Robomaster Development Board, type C, DJI), and a power supply placed in the base of the rigid arm.

Data analysis

The motor current, speed, and position data are captured using an STM32Cube monitor. The cable length is converted from the recorded rotor position of the motors in MATLAB. For dynamic tasks (as shown in **Figures 5** and **S11–S13**), videos and screenshots are captured using a high-speed camera (ACS-3, NAC Image Technology).

RESOURCE AVAILABILITY

Lead contact

Requests for further information and resources should be directed to and will be fulfilled by the lead contact, Nikolaos M. Freris (nfr@ustc.edu.cn).

Materials availability

Materials regarding the design and fabrication are shared.

Data and code availability

- This paper does not have any code to report.
- Any additional information required to reanalyze the data reported in this paper is available from the [lead contact](#) upon request.

ACKNOWLEDGMENTS

The authors would like to thank Dr. Juan Wang and Mr. Yiyuan Zhang for insightful discussions and experimental advice and Dr. Ye Tao (Bambu Lab Inc.) for providing the 3D printer. We also appreciate the Innovation Practice Base, the Information Science Center of USTC, Prof. Jianmin Ji, and Prof. Wei Gong for their support of experiments.

AUTHOR CONTRIBUTIONS

Conceptualization, Z.W. and N.M.F.; methodology, Z.W. and N.M.F.; investigation, Z.W., N.M.F., and X.W.; writing – original draft, Z.W. and N.M.F.; writing – review & editing, Z.W., N.M.F., and X.W.; supervision, N.M.F. and X.W.

DECLARATION OF INTERESTS

Z.W. and N.M.F. are listed as inventors on a Chinese patent (CN114770585B) that covers the fundamental principles and designs of SpiRobs.

SUPPLEMENTAL INFORMATION

Supplemental information can be found online at <https://doi.org/10.1016/j.device.2024.100646>.

Received: September 30, 2024

Revised: November 5, 2024

Accepted: November 18, 2024

Published: December 6, 2025

REFERENCES

1. Porter, M.M., Adriaens, D., Hatton, R.L., Meyers, M.A., and McKittrick, J. (2015). Why the seahorse tail is square. *Science* 349, aaa6683. <https://doi.org/10.1126/science.aaa6683>.
2. Luger, A.M., Ollevier, A., De Kegel, B., Herrel, A., and Adriaens, D. (2020). Is variation in tail vertebral morphology linked to habitat use in chameleons? *J. Morphol.* 281, 229–239. <https://doi.org/10.1002/jmor.21093>.
3. Kier, W.M., and Stella, M.P. (2007). The arrangement and function of octopus arm musculature and connective tissue. *J. Morphol.* 268, 831–843. <https://doi.org/10.1002/jmor.10548>.
4. Dagenais, P., Hensman, S., Haechler, V., and Milinkovitch, M.C. (2021). Elephants evolved strategies reducing the biomechanical complexity of their trunk. *Curr. Biol.* 31, 4727–4737.e4. <https://doi.org/10.1016/j.cub.2021.08.029>.
5. Kim, S., Laschi, C., and Trimmer, B. (2013). Soft robotics: a bioinspired evolution in robotics. *Trends Biotechnol.* 31, 287–294. <https://doi.org/10.1016/j.tibtech.2013.03.002>.
6. Rus, D., and Tolley, M.T. (2015). Design, fabrication and control of soft robots. *Nature* 521, 467–475. <https://doi.org/10.1038/nature14543>.
7. Hauser, H., and Hughes, J. (2024). Morphological computation—Past, present and future. *Device* 2, 100439. <https://doi.org/10.1016/j.device.2024.100439>.
8. Ilievski, F., Mazzeo, A.D., Shepherd, R.F., Chen, X., and Whitesides, G.M. (2011). Soft Robotics for Chemists. *Angew. Chem. Int. Ed.* 50, 1890–1895. <https://doi.org/10.1002/anie.201006464>.
9. Jiang, H., Wang, Z., Jin, Y., Chen, X., Li, P., Gan, Y., Lin, S., and Chen, X. (2021). Hierarchical control of soft manipulators towards unstructured interactions. *Int. J. Robot. Res.* 40, 411–434. <https://doi.org/10.1177/0278364920979367>.
10. Guan, Q., Stella, F., Della Santina, C., Leng, J., and Hughes, J. (2023). Trimmed helicoids: an architected soft structure yielding soft robots with high precision, large workspace, and compliant interactions. *npj Robot.* 1, 4. <https://doi.org/10.1038/s44182-023-00004-7>.
11. Burgner-Kahrs, J., Rucker, D.C., and Choset, H. (2015). Continuum Robots for Medical Applications: A Survey. *IEEE Trans. Robot.* 31, 1261–1280. <https://doi.org/10.1109/TRO.2015.2489500>.
12. Gaeta, L.T., Albayrak, M.D., Kinnicutt, L., Aufrichtig, S., Sultanian, P., Schlegel, H., Ellis, T.D., and Ranzani, T. (2024). A magnetically controlled soft robotic glove for hand rehabilitation. *Device* 2, 100512. <https://doi.org/10.1016/j.device.2024.100512>.
13. Wilson, J.F., Mahajan, U., Wainwright, S.A., and Croner, L.J. (1991). A Continuum Model of Elephant Trunks. *J. Biomech. Eng.* 113, 79–84. <https://doi.org/10.1115/1.2894088>.
14. Gutfreund, Y., Flash, T., Yarom, Y., Fiorito, G., Segev, I., and Hochner, B. (1996). Organization of Octopus Arm Movements: A Model System for Studying the Control of Flexible Arms. *J. Neurosci.* 16, 7297–7307. <https://doi.org/10.1523/JNEUROSCI.16-22-07297.1996>.
15. Kier, W.M., and Smith, K.K. (1985). Tongues, tentacles and trunks: the biomechanics of movement in muscular-hydrostats. *Zool. J. Linn. Soc.* 83, 307–324. <https://doi.org/10.1111/j.1096-3642.1985.tb01178.x>.
16. Grzesiak, A., Becker, R., and Verl, A. (2011). The Bionic Handling Assistant: a success story of additive manufacturing. *Assemb. Autom.* 31, 329–333. <https://doi.org/10.1108/01445151111172907>.
17. Nguyen, P.H., Sparks, C., Nutti, S.G., Vale, N.M., and Polygerinos, P. (2019). Soft Poly-Limbs: Toward a New Paradigm of Mobile Manipulation for Daily Living Tasks. *Soft Robot.* 6, 38–53. <https://doi.org/10.1089/soro.2018.0065>.
18. Xie, Z., Yuan, F., Liu, J., Tian, L., Chen, B., Fu, Z., Mao, S., Jin, T., Wang, Y., He, X., et al. (2023). Octopus-inspired sensorized soft arm for environmental interaction. *Sci. Robot.* 8, eadh7852. <https://doi.org/10.1126/scirobotics.adh7852>.
19. Coevoet, E., Escande, A., and Duriez, C. (2017). Optimization-Based Inverse Model of Soft Robots With Contact Handling. *IEEE Rob. Autom. Lett.* 2, 1413–1419. <https://doi.org/10.1109/LRA.2017.2669367>.
20. Morales Bieze, T., Kruszewski, A., Carrez, B., and Duriez, C. (2020). Design, implementation, and control of a deformable manipulator robot based on a compliant spine. *Int. J. Robot. Res.* 39, 1604–1619. <https://doi.org/10.1177/0278364920910487>.
21. Amanov, E., Nguyen, T.-D., and Burgner-Kahrs, J. (2021). Tendon-driven continuum robots with extensible sections—A model-based evaluation of

- path-following motions. *Int. J. Robot Res.* 40, 7–23. <https://doi.org/10.1177/0278364919886047>.
22. Calisti, M., Giorelli, M., Levy, G., Mazzolai, B., Hochner, B., Laschi, C., and Dario, P. (2011). An octopus-bioinspired solution to movement and manipulation for soft robots. *Bioinspiration Biomimetics* 6, 036002. <https://doi.org/10.1088/1748-3182/6/3/036002>.
23. Cianchetti, M., Arienti, A., Follador, M., Mazzolai, B., Dario, P., and Laschi, C. (2011). Design concept and validation of a robotic arm inspired by the octopus. *Mater. Sci. Eng. C* 31, 1230–1239. <https://doi.org/10.1016/j.msec.2010.12.004>.
24. Shepherd, R.F., Ilievski, F., Choi, W., Morin, S.A., Stokes, A.A., Mazzeo, A.D., Chen, X., Wang, M., and Whitesides, G.M. (2011). Multigait soft robot. *Proc. Natl. Acad. Sci. USA* 108, 20400–20403. <https://doi.org/10.1073/pnas.1116564108>.
25. Paek, J., Cho, I., and Kim, J. (2015). Microrobotic tentacles with spiral bending capability based on shape-engineered elastomeric microtubes. *Sci. Rep.* 5, 10768. <https://doi.org/10.1038/srep10768>.
26. Xie, Z., Domel, A.G., An, N., Green, C., Gong, Z., Wang, T., Knubben, E.M., Weaver, J.C., Bertoldi, K., and Wen, L. (2020). Octopus Arm-Inspired Tapered Soft Actuators with Suckers for Improved Grasping. *Soft Robot.* 7, 639–648. <https://doi.org/10.1089/soro.2019.0082>.
27. Zhang, J., Hu, Y., Li, Y., Ma, K., Wei, Y., Yang, J., Wu, Z., Rajabi, H., Peng, H., and Wu, J. (2022). Versatile Like a Seahorse Tail: A Bio-Inspired Programmable Continuum Robot For Conformal Grasping. *Adv. Intell. Syst.* 4, 2200263. <https://doi.org/10.1002/aisy.202200263>.
28. Taylor, I.H., Bawa, M., and Rodriguez, A. (2023). A Tactile-enabled Hybrid Rigid-Soft Continuum Manipulator for Forceful Enveloping Grasps via Scale Invariant Design. In IEEE International Conference on Robotics and Automation (ICRA), pp. 10331–10337. <https://doi.org/10.1109/ICRA48891.2023.10161121>.
29. Rothemund, P., Ainla, A., Belding, L., Preston, D.J., Kurihara, S., Suo, Z., and Whitesides, G.M. (2018). A soft, bistable valve for autonomous control of soft actuators. *Sci. Robot.* 3, eaar7986. <https://doi.org/10.1126/scirobotics.aar7986>.
30. Zhang, Z., Wang, X., Meng, D., and Liang, B. (2021). Bioinspired Spiral Soft Pneumatic Actuator and Its Characterization. *J. Bionic Eng.* 18, 1101–1116. <https://doi.org/10.1007/s42235-021-00075-y>.
31. Grissom, M.D., Chitrakaran, V., Dienno, D., Csencits, M., Pritts, M., Jones, B., McMahan, W., Dawson, D., Rahn, C., and Walker, I. (2006). Design and experimental testing of the OctArm soft robot manipulator. In SPEI Unmanned systems technology VIII, pp. 491–500. <https://doi.org/10.1117/12.665321>.
32. Jiang, H., Liu, X., Chen, X., Wang, Z., Jin, Y., and Chen, X. (2016). Design and simulation analysis of a soft manipulator based on honeycomb pneumatic networks. In IEEE International Conference on Robotics and Biomimetics (ROBIO), pp. 350–356. <https://doi.org/10.1109/ROBIO.2016.7866347>.
33. Thompson, D.W. (1992). In On Growth and Form, 1st ed., J.T. Bonner, ed. (Cambridge University Press). <https://doi.org/10.1017/CBO9781107325852>.
34. Porter, M.M., Novitskaya, E., Castro-Ceseña, A.B., Meyers, M.A., and McKittrick, J. (2013). Highly deformable bones: Unusual deformation mechanisms of seahorse armor. *Acta Biomater.* 9, 6763–6770. <https://doi.org/10.1016/j.actbio.2013.02.045>.
35. Hammer, Ø. (2016). The Perfect Shape (Springer International Publishing). <https://doi.org/10.1007/978-3-319-47373-4>.
36. Webster, R.J., and Jones, B.A. (2010). Design and Kinematic Modeling of Constant Curvature Continuum Robots: A Review. *Int. J. Robot Res.* 29, 1661–1683. <https://doi.org/10.1177/0278364910368147>.
37. Todorov, E., Erez, T., and Tassa, Y. (2012). MuJoCo: A physics engine for model-based control. In IEEE/RSJ International Conference on Intelligent Robots and Systems, pp. 5026–5033. <https://doi.org/10.1109/IROS.2012.6386109>.
38. Packard, A., and Sanders, G.D. (1971). Body patterns of Octopus vulgaris and maturation of the response to disturbance. *Anim. Behav.* 19, 780–790. [https://doi.org/10.1016/S0003-3472\(71\)80181-1](https://doi.org/10.1016/S0003-3472(71)80181-1).
39. Hirose, S., and Umetani, Y. (1978). The development of soft gripper for the versatile robot hand. *Mech. Mach. Theor.* 13, 351–359. [https://doi.org/10.1016/0094-114X\(78\)90059-9](https://doi.org/10.1016/0094-114X(78)90059-9).
40. Ruotolo, W., Brouwer, D., and Cutkosky, M.R. (2021). From grasping to manipulation with gecko-inspired adhesives on a multifinger gripper. *Sci. Robot.* 6, eabi9773. <https://doi.org/10.1126/scirobotics.abi9773>.
41. Becker, K., Teeple, C., Charles, N., Jung, Y., Baum, D., Weaver, J.C., Mahadevan, L., and Wood, R. (2022). Active entanglement enables stochastic, topological grasping. *Proc. Natl. Acad. Sci. USA* 119, e2209819119. <https://doi.org/10.1073/pnas.2209819119>.
42. Zournatzis, I., Kalaitzakis, S., and Polygerinos, P. (2023). SOFTER: A Spiral Soft Robotic Ejector for Sorting Applications. *IEEE Robot. Autom. Lett.* 8, 7098–7105. <https://doi.org/10.1109/LRA.2023.3315206>.
43. Wang, W., Li, C., Cho, M., and Ahn, S.-H. (2018). Soft Tendril-Inspired Grippers: Shape Morphing of Programmable Polymer–Paper Bilayer Composites. *ACS Appl. Mater. Interfaces* 10, 10419–10427. <https://doi.org/10.1021/acsami.7b18079>.
44. Henrich, A. (2021). John Edmark: Art in Motion. *Math. What Mag.* 94, 65–68. <https://doi.org/10.1080/0025570X.2021.1843890>.
45. Sugiura, S., Unde, J., Zhu, Y., and Hasegawa, Y. (2023). High-strength and flexible mechanism for body weight support. *Robomech J.* 10, 16. <https://doi.org/10.1186/s40648-023-00255-x>.
46. Glick, P.E., Van Crey, N., Tolley, M.T., and Ruffatto, D. (2020). Robust capture of unknown objects with a highly under-actuated gripper. In IEEE International Conference on Robotics and Automation (ICRA), pp. 3996–4002. <https://doi.org/10.1109/ICRA40945.2020.9197100>.
47. Wang, Z., and Freris, N.M. (2024). Exploiting Frictional Effects to Reproduce Octopus-Like Reaching Movements with a Cable-Driven Spiral Robot. In IEEE International Conference on Soft Robotics (RoboSoft), pp. 537–542. <https://doi.org/10.1109/RoboSoft60065.2024.10522036>.
48. Schulz, A.K., Boyle, M., Boyle, C., Sordilla, S., Rincon, C., Hooper, S., Aubuchon, C., Reidenberg, J.S., Higgins, C., and Hu, D.L. (2022). Skin wrinkles and folds enable asymmetric stretch in the elephant trunk. *Proc. Natl. Acad. Sci. USA* 119, e2122563119. <https://doi.org/10.1073/pnas.2122563119>.

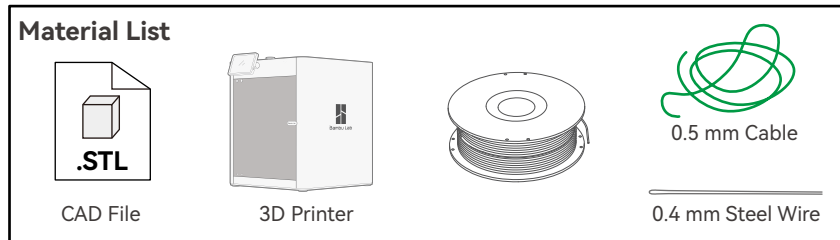
DEVICE, Volume 3

Supplemental information

**SpiRobs: Logarithmic spiral-shaped robots
for versatile grasping across scales**

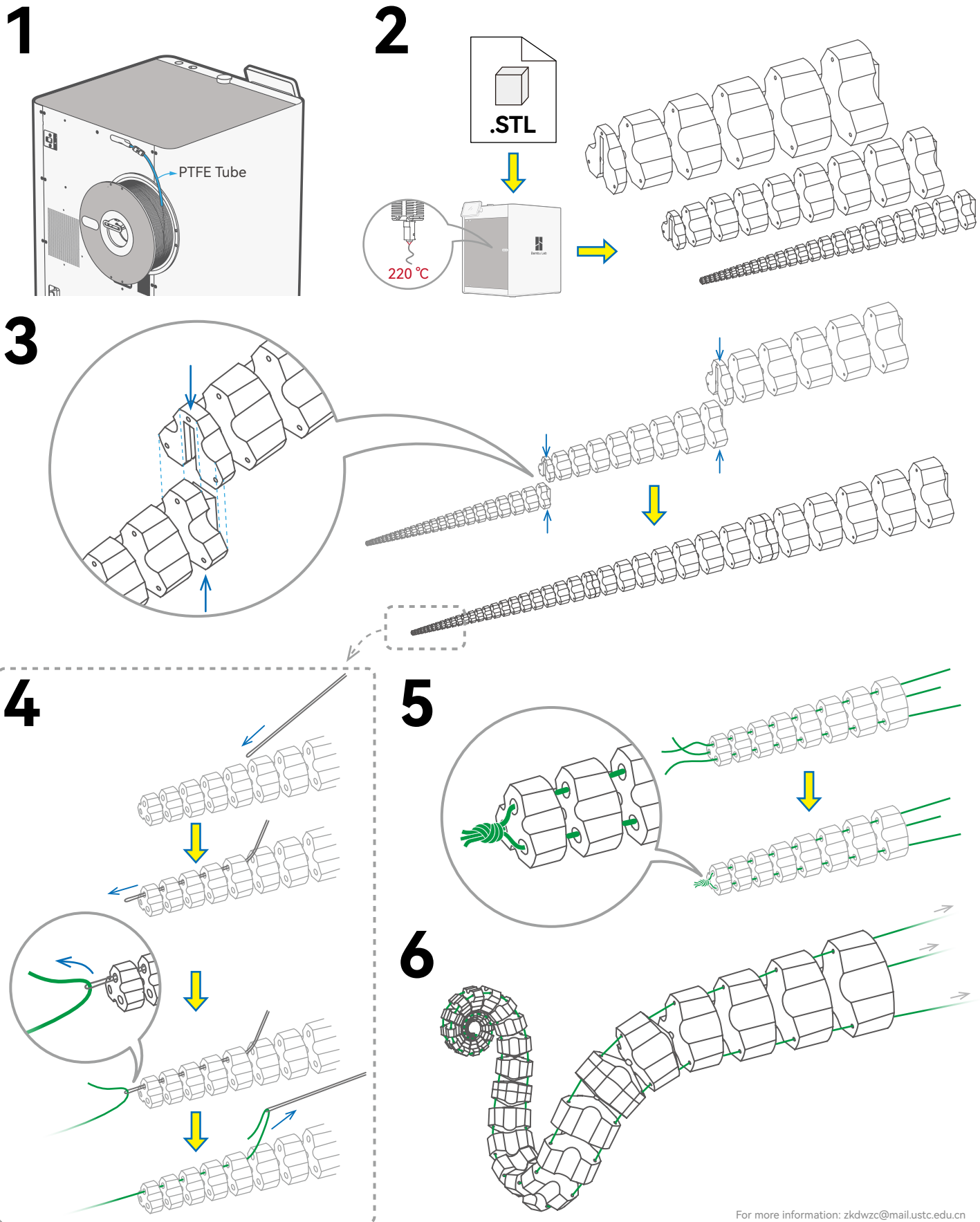
Zhanchi Wang, Nikolaos M. Freris, and Xi Wei

Supplemental Experimental Procedures



SpiRob

Fabrication Instructions



Supplemental Notes

Note S1. Fabrication of SpiRobs

The main body of the SpiRob is printed with Thermoplastic Polyurethane (TPU) using a Bambu Lab X1CC printer. Here are some important points to consider when printing:

- **Choose TPU with the appropriate hardness.** Different hardness levels of TPU will result in different robot stiffness. For example, there are options like 68D, 95A, and 83A (listed in descending order of hardness). We used eTPU 95A from eSUN Inc. because it ensures high printing quality (lower hardness levels have a higher risk of printing failure).
- **Keep TPU filament dry before use.** Dry the filament to prevent moisture-related issues like excessive stringing or oozing in the resulting prototype.
- **Feed TPU filament smoothly into the printer.** When using the 3D printer, do not use the Automated Material System (AMS). Instead, place the TPU directly on the rear spool holder or an external holder (see Supplemental Experimental Procedures for details). Ensure that the material spool turns smoothly to reduce resistance when feeding the material to the extruder.

We have included a .3mf file with the settings used for printing TPU. For more information on printing TPU filament, please refer to Bambu Lab's printing guide.

After printing, pass the cables through the robot (see Supplemental Experimental Procedures). You can use a 0.5 mm diameter UHMWPE (ultra-high molecular weight polyethylene) cable because it is soft, durable, and does not stretch easily. As the size of the units gets smaller towards the tip, the holes also become smaller, making it difficult to pass the cable through them. For this reason, use a stiffer, thinner steel wire to create a needle-like tool that helps guide the cable through the small holes (see Supplemental Experimental Procedures for a visualization). Afterwards, tie a knot at the tip of the robot and connect the other end of the cables to motors to drive the robot's movement.

In addition to the 3D printing method, we demonstrate a method for Origami fabrication of the robot using a sheet of paper (Figure S2D). The idea is to expand the body of the robot on a plane. Thanks to the proportional relationship between adjacent units, we can obtain the design of the entire robot from a two-dimensional expanded view of one unit. This method is similar to building Origami toys, in which the pattern printed on the paper needs to be cut out, bent, and glued in place. There is no specific design of an elastic layer, and the inner portion of the paper sheet serves this role. We demonstrate that the robot can grasp an apple (170 g, 34 times its self-weight) even when made with a sheet of paper (5 g). A 2-cable robot made in a similar way is shown in Figure S2E, comprising two 1-cable robots built separately and glued together. This Origami method is suitable for making 1- or 2- cable prototypes. It is difficult to fabricate 3-cable robots (capable of torsional deformations) this way.

Note S2. Theoretical characterization of spiral robots

This section describes the theoretical analysis of the spiral robot's workspace, grasping range,

and load capacity. We take a 2-cable robot as an example for illustration. The workspace envelope can be obtained through the following process: each robot unit rotates from the one closest to the base, one joint at a time, while the other units are maintained as a straight line during the rotation process. Consequently, the envelope can be characterized by serially connected arcs drawn by the tip at each stage of the rotation process (Figures 2E and S4A). It is, therefore, approximately captured by the involute of the central spiral (ρ_c), which is another logarithmic spiral (ρ_w , see Figure S4B):

$$\rho_w = \frac{a}{2b} (e^{2\pi b} + 1) e^{b(\theta - \frac{\pi}{2})}.$$

We can infer that the larger b is (i.e., larger taper angle ϕ , as can be seen by taking the derivative in (3) to establish that ϕ is increasing in b), the faster the change of radius with angle, and thus the smaller the working space (obtained by varying $\theta \in [0, \theta_0]$): this is in alliance with our simulation results (Figure 2E), which further attest that all points inside the envelope are reachable (the points in Figure 2E are obtained by inputting random control signals and recording the trajectory of the tip). This contrasts sharply with existing soft robots whose workspace is limited by the deformation rate, resulting in an almost spherical shell-like region^[S1].

To study the effect of the discretization, we consider the difference in swept area between the multi-unit robot based on discretization (S_1) and a continuous spiral-shaped body (S_2) (see Figure S4A and B):

$$S_1 = L(\theta) \Delta\theta, \quad S_2 = \int_{\theta-\Delta\theta}^{\theta} L(\theta) d\theta, \quad (10)$$

$$\eta = \frac{S_2}{S_1} = \frac{1}{b} \left(\frac{1-e^{-b\Delta\theta}}{\Delta\theta} \right). \quad (11)$$

In particular, note that η is independent of θ . This establishes a uniformly bounded approximation error, which goes to 0 ($\eta \rightarrow 1$) as $\Delta\theta \rightarrow 0$. This analysis was carried out for the 'virtual' tip (where two outer contours of the robot meet, i.e., $\theta \rightarrow -\infty$) solely for notational simplification.

After grasping the object, the workspace can also be analyzed using a similar geometric approach (Figure S4C). The idea is to regard grasping as a loss of a portion of the effective length. To calculate this loss, we consider the central axis of the portion used to grasp the object (the blue dashed line around the object in Figure S4D), which is a spiral characterized by:

$$\rho'_c(\theta, d) = \frac{d+\delta(0)}{2} e^{\cot \frac{\pi-\phi}{2} \theta}, \quad (12)$$

where the tangential angle is $\frac{\pi-\phi}{2}$ and $\delta(0)$ is the width of the tip. The length required to grasp an object with a diameter of d (assuming the object is circular and the robot wraps a fraction n of the circumference; $n \geq 50\%$ is taken as the lower bound for wrapping to grasp the object) is given by:

$$L_{\text{grasp}} = \int_0^{2\pi n} \sqrt{{\rho'_c}^2 + {\dot{\rho}'_c}^2} d\theta. \quad (13)$$

The remaining length is $L' = L - L_{\text{grasp}}$. By fixing L' and repeating the analysis procedure, we

obtain the workspace envelope after grasping the object: it approximately follows another logarithmic spiral.

As for the size that can be grasped, the theoretical minimum diameter is $d_{\min} = \rho(0) + \rho(\pi) = a + ae^{b\pi}$, which corresponds to the diameter of the inscribed circle when the robot is packed into a spiral. For fixed width of the tip $\delta(0)$, a constraint is introduced between a and b as

$$a = \frac{\delta(0)}{e^{2\pi b} - 1}, \text{ which further implies:}$$

$$d_{\min} = \frac{\delta(0)(e^{\pi b} + 1)}{e^{2\pi b} - 1}. \quad (14)$$

The maximum diameter that can theoretically be grasped satisfies the following equation (Table S1):

$$L = \int_0^\pi \sqrt{\rho'_c(\theta, d_{\max})^2 + \dot{\rho}'_c(\theta, d_{\max})^2} d\theta. \quad (15)$$

This can be translated as the full length of the robot used to wrap 1/2 of the object's circumference (deemed as the bare minimum for grasping by wrapping). From (14) and (15), it can be inferred that the larger b is (which corresponds to a larger taper angle; see (3)), the smaller the maximum/minimum diameter of an object that the robot can grasp.

In reference to the load that can be grasped, we consider the situation shown in Figure S4C, where the cable force has reached its maximum value. In this case, increasing the object's diameter or its mass (or both) will cause the grasp to fail. This can be analyzed by means of torque balance:

$$M_{\max} g \rho'_c(\pi, d) = F_{\max} \left(\rho'_c(\pi, d) - \frac{d}{2} \right), \quad (16)$$

where the left side is the gravitational torque that aims to unfold the robot, and the right is the actuation torque. Based on (12), (14), and (15), we can derive the relationship between the taper angle and the mass/diameter of the grasped object (the expression is shown in Table S1, and the results are plotted in Figure 2F). Note that, to simplify the analysis, we ignore the elastic force exerted from the elastic layer, the friction between the cable and the body, and the deformation of the units: the extreme case analyzed here is thus a theoretical upper bound on the load value.

Note S3. Modeling and simulation

To analyze the kinematic and dynamic behavior, we adopt the mechanism of a serial elastic joint (i.e., a series of links connected by joints) to simulate the spiral robot in MuJoCo (Figure S5A). For 2-cable robots, which can only bend on a plane, the adjacent units are connected with 1-DOF (degree of freedom) revolute joints. For 3-cable robots capable of deforming in the 3D space, we use 3-DOF ball joints to connect adjacent units (Figure S5B). The simulation of the cable-actuation mechanism uses the tendon-muscle class provided by MuJoCo. The viscoelasticity of the joints in the simulation is estimated directly from the material and geometric properties of the real robot (for example, the joint stiffness can be calculated from Young's modulus and the geometry of the elastic layer connecting the units). Note that since the adjacent units are proportional in scale, we only need to determine the parameters of one

link/joint (size, mass, viscosity, and elasticity), and the rest are derived by proportionality. For example, the ratio of mass is the third power of the ratio of unit length (assuming uniform density). It is critical to introduce limits for the robot joints in the simulation: correspond to a unit touching the next unit, i.e., are equal to $\pm\Delta\theta$. In particular, when all joints reach their upper/lower bound limits simultaneously, the robot is tightly packed into a logarithmic spiral.

Note S4. Evaluation of the bioinspired grasping strategy

Recall that our strategy is inspired by the octopus and consists of the following stages: extending the curled arms toward the object (*Reaching*), making contact with the object, and uncurling the arms along the surface to wrap around (*Wrapping*, Figure 3A, Video S3). We reproduce this strategy by controlling the cable forces. To verify its effectiveness, we conducted comparative experiments when this strategy was on or off (see Figure S6). When off, as the cable force increases, the robot starts to curl from the tip so that only objects within a limited range (close to the tip) can be successfully grasped. Objects at a larger (but still reachable) range will be missed (Figure S6A). In contrast, using the proposed bioinspired strategy, the robot can spread its tightly packed body in different directions and successfully wrap to grasp objects (Figure S6B). In addition, we quantitatively studied the grasping space of different-sized objects (Figure 3C). It is worth noting, in passing, that the sucker of the octopus also plays a very important role in grasping (complementary to wrapping); here, we only focus on reproducing the wrapping behavior and defer exploring the addition of suction cups to future work.

Note S5. Manipulating various objects

We use a 2-cable SpiRob (45cm in length) to demonstrate the ability to grasp and manipulate various objects. We tested for numerous objects varying in size, shape, and weight. We show that the same robot with the same strategy can successfully grasp and manipulate various objects (see Figure S7 and Video S6). Since visual perception and control were not the focus of these experiments, we manually controlled the two cables like a puppet.

We also tested the robot's ability to manipulate in confined spaces. The robot was used to move a pingpong to a designated position (Figure S8). The "Wrapping" behavior exhibited by the robot allows it to move on surfaces of varying roughness, turn around, and traverse a slit (Figure S8, Video S7).

Note S6. Remote control for the drone application

We built a control terminal for human teleoperation (Figures 5 and S2), which consists of three motors (M2006, DJI) and an embedded controller (Robomatser Development Board, type C, DJI). The terminal communicates with a joystick through a 2.4 GHz wireless channel and converts the commands into reference torque signals fed to the motors.

Supplemental Tables:

Table S1. Parameters for the design of a two-cable SpiRob

Parameter	Symbol	Parameterized expression
Polar coordinate	θ	-
Scaling factor	a	-
Scaling factor	b	-
Discretization step	$\Delta\theta$	-
Logarithmic spiral	$\rho(\theta)$	$ae^{b\theta}$
Central spiral	$\rho_c(\theta)$	$\frac{a}{2}(e^{2\pi b} + 1)e^{b\theta}$
Length of the central spiral from angle θ_1 to θ_2	$L(\theta_1, \theta_2)$	$\int_{\theta_1}^{\theta_2} \sqrt{\rho_c^2 + \dot{\rho}_c^2} d\theta = \frac{\sqrt{b^2 + 1}}{b} (\rho_c(\theta_2) - \rho_c(\theta_1))$
Length of the robot	$L(0, \theta_0)$	$L(0, \theta_0) = \frac{a\sqrt{b^2 + 1}}{2b} (e^{2\pi b} + 1) (e^{b\theta_0} - 1)$
Curvature at angle θ when packed into a spiral	$\kappa(\theta)$	$\frac{1}{\rho_c \sqrt{b^2 + 1}}$
Radius of curvature at s ($s \equiv L(-\infty, \theta)$)	$r(s)$	bs
Taper angle of the robot	ϕ	$2 \arctan\left(\frac{b(e^{2\pi b} - 1)}{\sqrt{b^2 + 1}(e^{2\pi b} + 1)}\right)$
Width of the robot at angle θ	$\delta(\theta)$	$ae^{b(\theta+2\pi)} - ae^{b\theta}$
Ratio between adjacent units	β	$e^{b\Delta\theta}$
Involute of the central spiral (workspace)	ρ_w	$\rho_w = \frac{a}{2b} (e^{2\pi b} + 1) e^{b(\theta - \frac{\pi}{2})}$
Minimum diameter of an object that can be grasped	d_{\min}	$a(1 + e^{b\pi})$
Maximum diameter of an object that can be grasped	d_{\max}	$L = \int_0^\pi \sqrt{\rho'_c(\theta, d_{\max})^2 + \rho''_c(\theta, d_{\max})^2} d\theta$
Maximum load that the robot can hold (with diameter d)	$M(\phi, d, F_{\max})$	$\frac{F_{\max}}{g} \left(1 - \frac{d}{(d + \delta(0)) e^{\cot(\frac{\pi - \phi}{2}) \pi}} \right)$

Table S2. Success rate of multi-SpiRob grasping (5 tests for each case)



Objects	2-SpiRob array	4-SpiRob array	6-SpiRob array	8-SpiRob array
①	2/5	5/5	3/5	5/5
②	3/5	5/5	5/5	5/5
③	3/5	3/5	5/5	5/5
④	5/5	5/5	5/5	5/5
⑤	5/5	5/5	5/5	5/5
⑥	1/5	0/5	5/5	1/5
⑦	2/5	4/5	5/5	5/5
⑧	1/5	1/5	3/5	5/5
⑨	4/5	5/5	5/5	5/5
⑩	2/5	3/5	5/5	5/5
Average±SD	0.48±0.23	0.72±0.37	0.92±0.17	0.94±0.19

Supplemental figures:

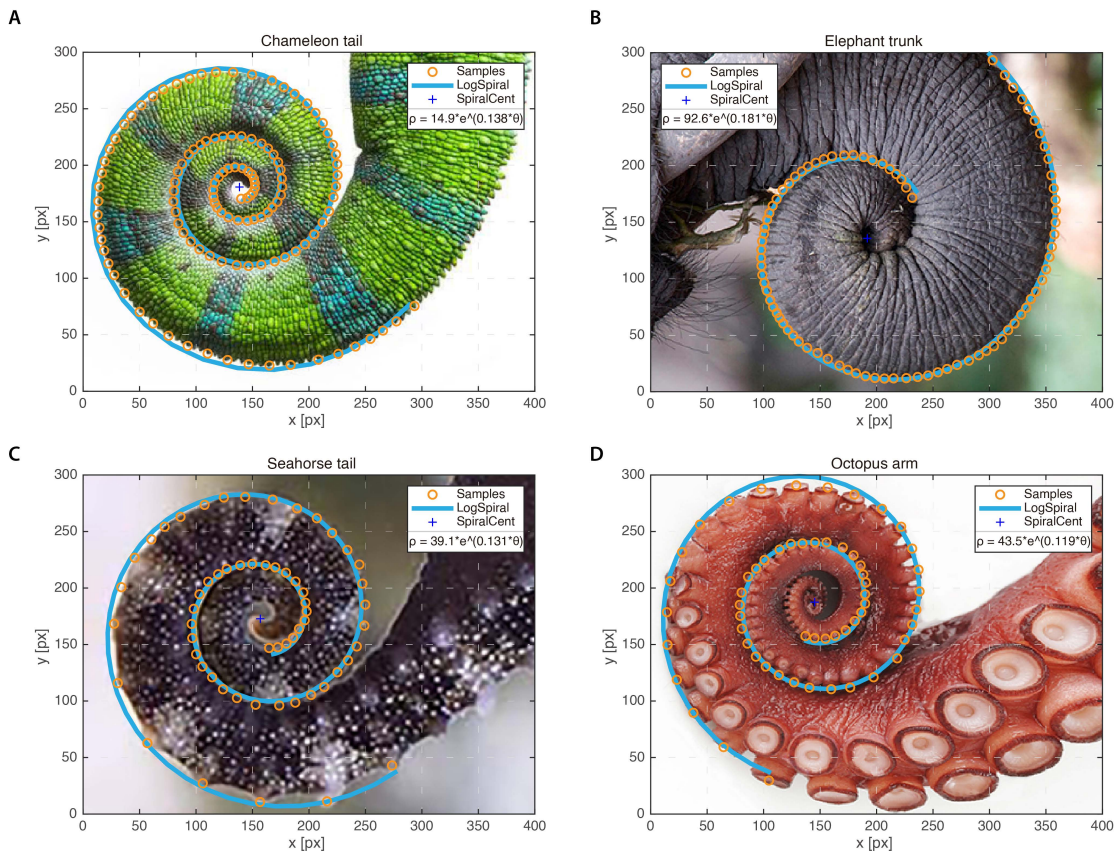


Figure S1. Logarithmic spirals in nature. (A)-(D) Fitting a logarithmic spiral to the chameleon tail, elephant trunk, seahorse tail, and octopus arm. The fitted parameters are shown for each case. We first cropped the image to 400x300 pixels and extracted points along the edges, then applied least squares fitting. All the pictures are from the Internet and were chosen so that the camera is perpendicular to the object to reduce the error caused by perspective.

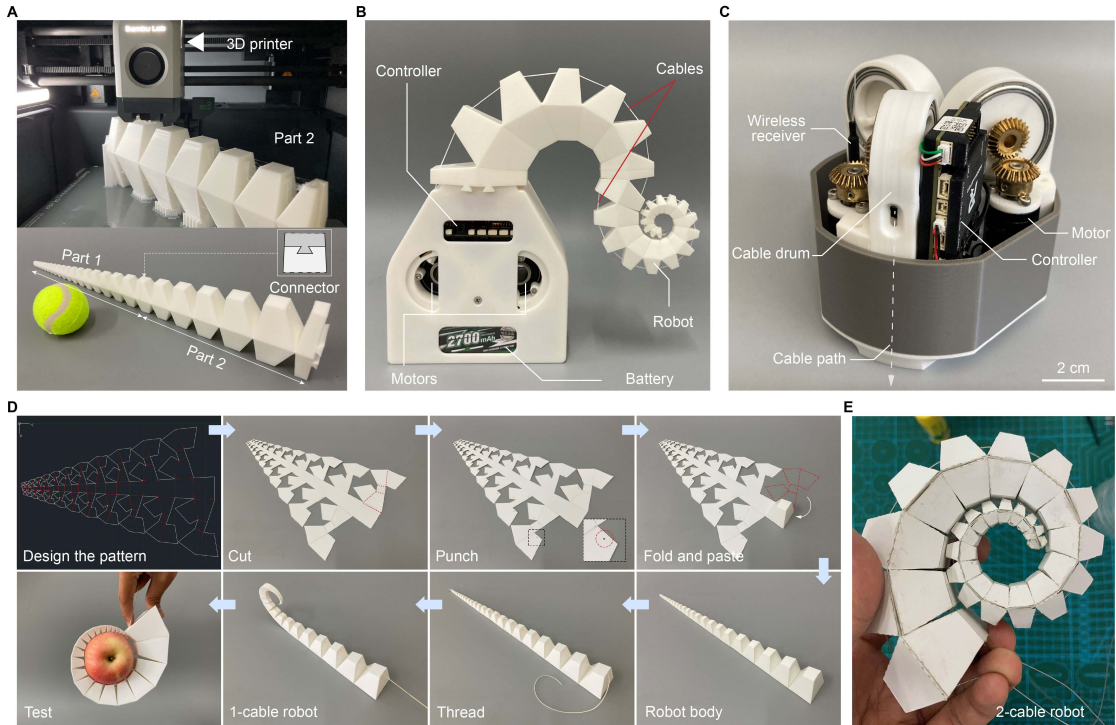


Figure S2. Fabrication and assembly of robot components. **(A)** Fabrication of robot body by 3D printing (first panel). Robots with different lengths can be obtained by printing parts separately and assembling them using connectors (dovetail shown in the second panel). **(B)** Hardware for driving a 2-cable SpiRob. The cables pass through the holes designed in each unit and are connected to DC motors. **(C)** The control terminal for 3-cable SpiRobs consists of three motors and an embedded controller. **(D)** Origami fabrication of SpiRobs. We first expanded the 3D model on a 2D plane, and then the robot was obtained by cutting, folding, and pasting a sheet of paper. We punch holes in the corresponding positions for the cable to pass. The spiral robots fabricated by this method are extremely light and can obtain a high load-to-weight ratio, but the maximum weight that can be grasped is, of course, smaller than robots made by 3D printing. **(E)** Picture of a 2-cable Origami SpiRob. Two 1-cable robots are glued back-to-back. The paper connecting the units constitutes the elastic layer.

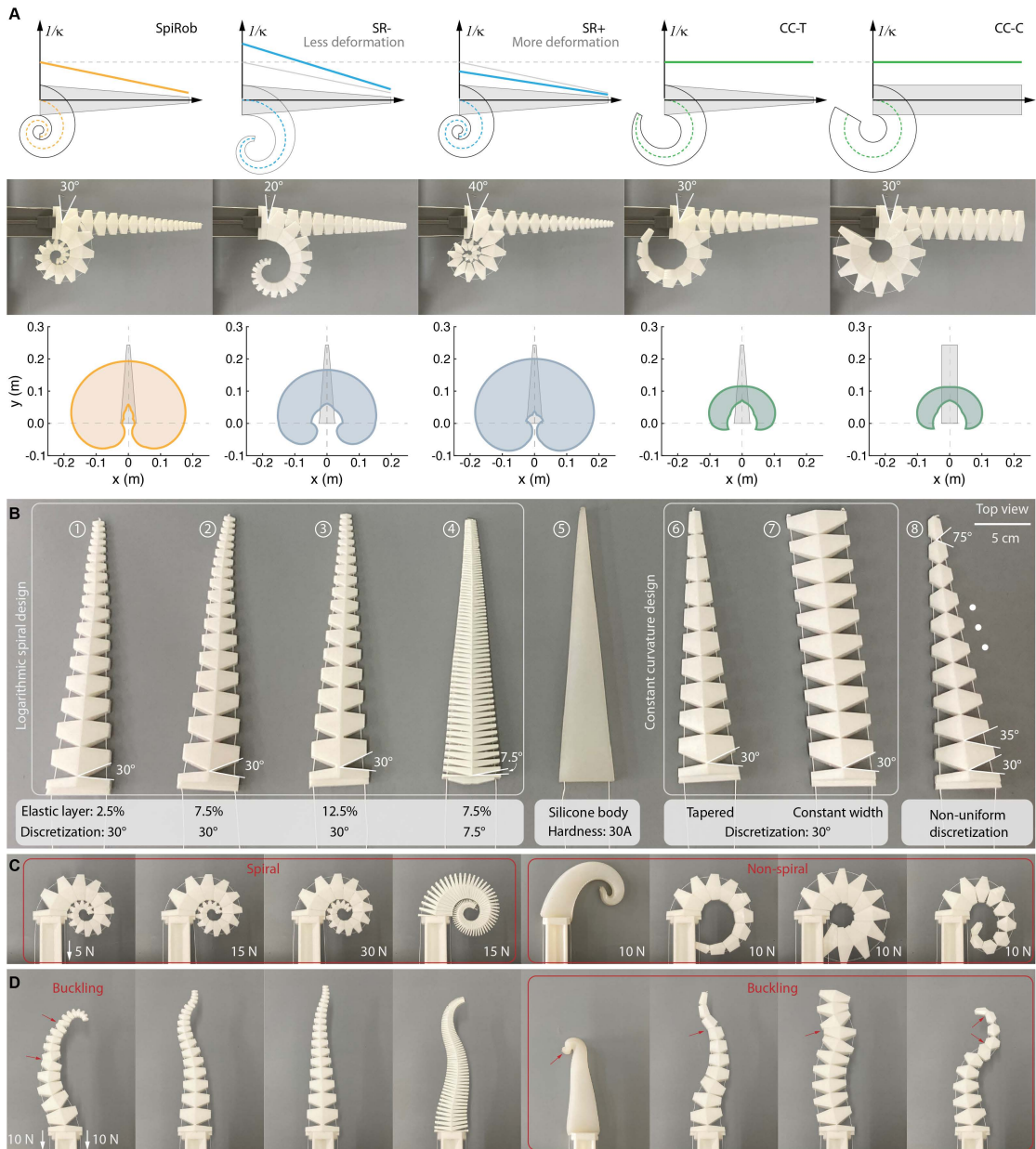


Figure S3. Comparison of different designs. (A) Prototypes for comparative experiments. SR- and SR+ are variants of our design with decreased/increased deformation ability (obtained by decreasing/ increasing the gaps by 10° while maintaining nominal lengths for each unit). CC-T is a tapered constant curvature robot^[S2], and CC-C is a cylindrical constant curvature robot. The workspaces for each of the different designs when holding the smallest graspable object are also plotted. **(B)** Prototypes of different SpiRobs (①-④) and non-spiral designs (⑤-⑧). **(C)** The cable is pulled on the right, and the actuation forces are marked in the lower right corner. For SpiRobs, the reported force is the minimum to attain tight packing. For non-spiral designs, the force is set as 10 N, and it is apparent from the visualization that they fail to achieve tight packing. **(D)** Applying antagonistic forces on the cables (10 N). For SpiRobs, thinner layers are easier to buckle (①). Smaller discretization steps can relieve buckling (④), but the fabrication is more challenging because units closer to the tip are getting smaller. Non-spiral designs tend to exhibit severe buckling under antagonistic forces.

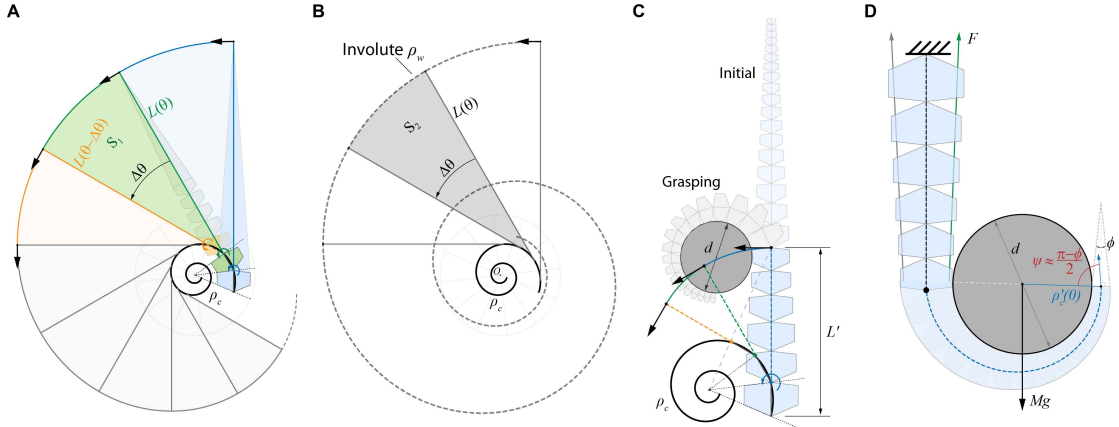


Figure S4. Workspace and load analysis. **(A)** Starting from the base, we progressively turn the joint of each unit until it touches the next unit. The tip draws arcs (illustrated as blue, green, and orange); this gives a piecewise arc approximation of the involute spiral. **(B)** The involute spiral (ρ_w) approximately captures the envelope of the workspace. **(C)** With a similar approach, we can analyze the envelope when grasping an object. In this case, the point of interest is no longer the robot's tip but a point on the robot's body. L' is the length of the robot after grasping. **(D)** Load capacity analysis. We consider an object of fixed diameter d for increasing weight until the robot cannot wrap around more than 1/2 of its circumference (deemed a grasping failure). In this critical state, a torque balance between the actuation force (F) and the weight of the object (Mg) is achieved. This determines a theoretical upper bound on the maximum load capacity.

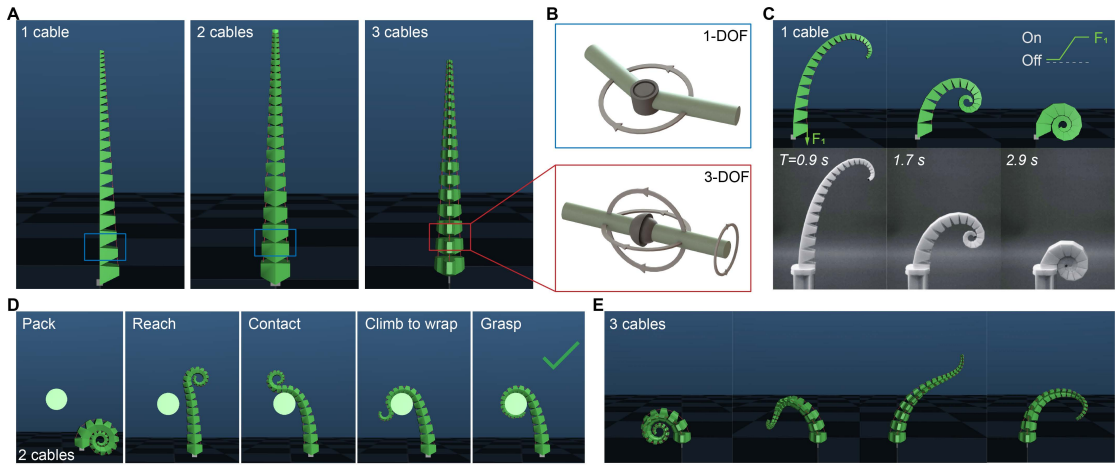


Figure S5. Simulation of spiral robots. **(A)** Images of 1-cable, 2-cable, and 3-cable SpiRobs in simulation. The first two are modeled using a series of 1-DOF revolute joints that connect the units, while the last uses 3-DOF ball joints (as shown in **(B)**). The rotational limits of the joints are set equal to the step size of the discretization (this corresponds to two adjacent units touching each other). The robot is completely packed into a logarithmic spiral when all joints have reached their limits. **(C)** Simulation (first panel) and demonstration (second panel) of the curling of the 1-cable robot. In this scenario, the actuation force of one cable (F_1) is gradually increased until packing is attained. **(D)** Image sequences show the effectiveness of the grasping strategy in simulation. **(E)** Image sequences showing the 3D deformation of a 3-cable SpiRob in various configurations.

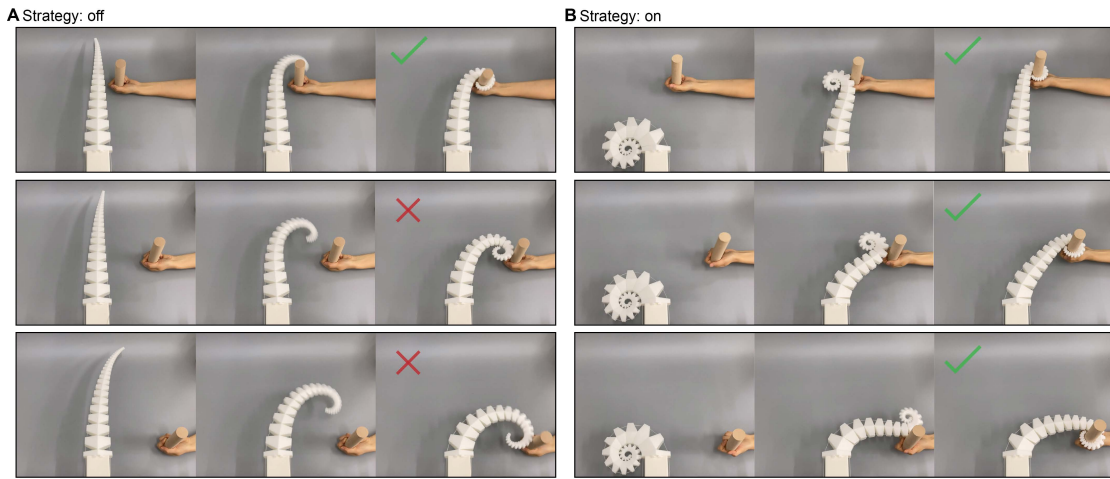


Figure S6. Bioinspired grasping strategy. (A) (B) Experiments to verify its effectiveness (Strategy: on) and comparison with a direct grasping attempt (Strategy: off). When the strategy is not used, the robot's grasping range is substantially limited ((A), second and third attempts fail). With the bioinspired strategy (B), the robot can reach out in different directions and climb along the surface of the objects to wrap and grasp them.

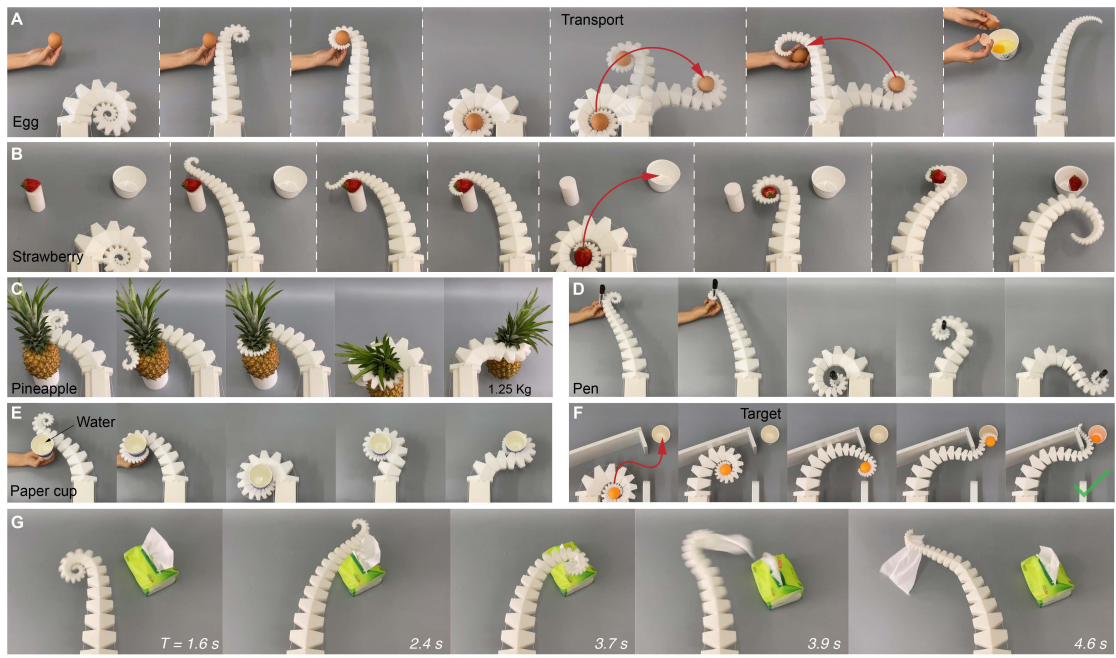


Figure S7. SpiRobs grasping and transporting various objects. (A)-(E) Image sequences of a 2-cable SpiRob handing a raw egg, a strawberry, a pineapple, a pen, and a paper cup filled with water. (F) The robot navigates through a door to transport a pingpong ball to its target in an S-shape trajectory. (G) SpiRob extracts tissue from a box resting on a table.

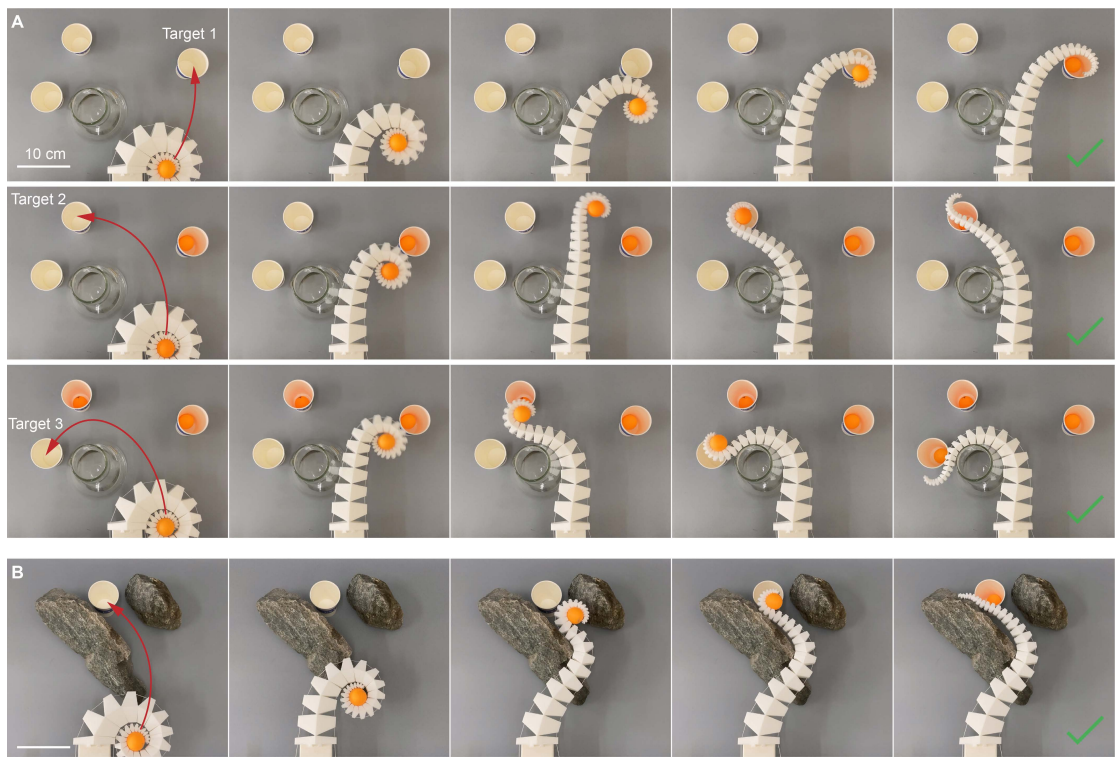


Figure S8. Manipulation in confined spaces. **(A)** Image sequences of the robot moving around a glass bottle to transport a pingpong ball to different targets. **(B)** The robot climbs on a rough stone surface and navigates through the two stones to drop the ball into the cup. These experiments were done by manually operating the two cables.

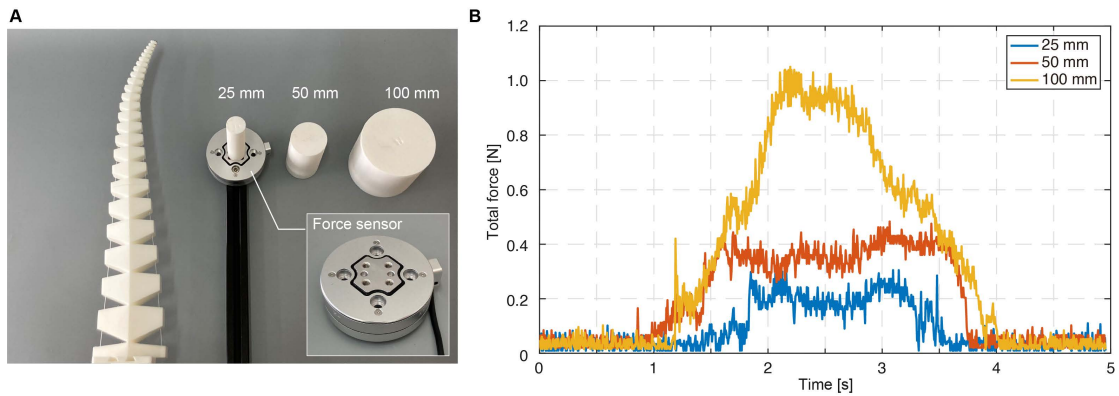


Figure S9. Contact force. **(A)** Experimental setup for measuring contact forces when the robot is climbing on the surface of an object. Objects of different diameters are placed on a force sensor (M4313A, SRI Inc.). **(B)** Measured force across time. The experimental results confirm that the wrapping process exerts force on the object, but the value remains low (and smaller for small objects).

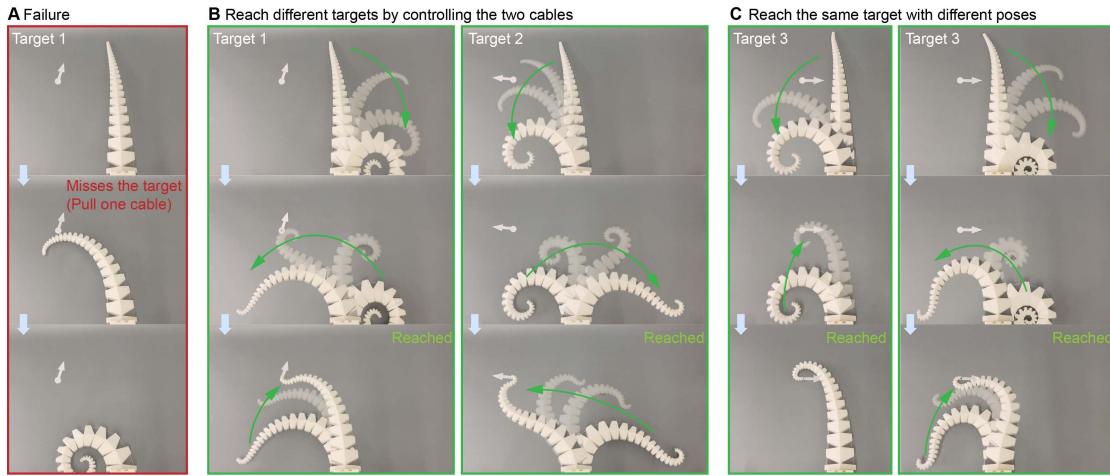


Figure S10. Controllability of the tip. **(A)** When only one cable is pulled, the whole robot's body curls and it is almost impossible to control the tip accurately to reach a target (target position and orientation are depicted with a solid white point and arrow). **(B)** By controlling two cables at the same time, different targets can be reached. The same goal can be reached with multiple poses **(C)**.

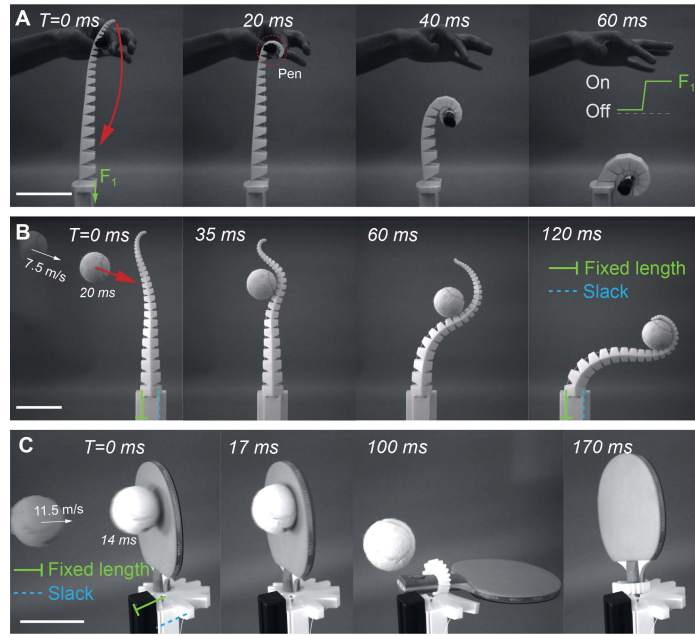


Figure S11. Dynamic grasping. **(A)** The robot grasps a pen and moves it to its base within 0.06s. The actuation pattern is displayed in the upper right corner where 'On' means the cable is stretched and 'Off' means the cable is slack. **(B)** Passive grasping. The robot can grasp a high-speed moving object within 120 ms without any control (the left cable is fixed to maintain a constant length while the right cable is slack). **(C)** The robot achieves a firm grasp of a pingpong racket, as demonstrated by throwing a tennis ball at high speed. Scale bars in (A)-(C) represent 10 cm.

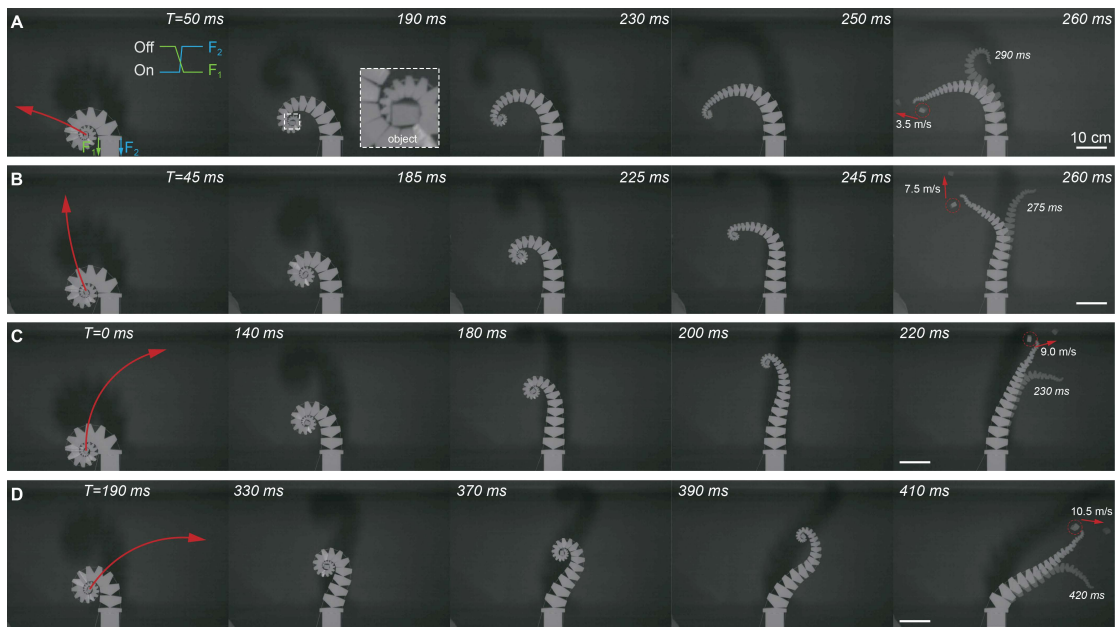


Figure S12. Elephant throw. (A)-(D) Image sequences of the robot throwing a piece of rubber in different directions. The robot starts from an initial state of wrapping the object and throws it out via an uncurling motion. Because of the rotation generated during the movement, the object flies out with a spin. From top to bottom, we observe that the longer the distance the robot moves with the object, the higher the velocity the object can obtain, with the highest release speed exceeding 10 m/s (D). Controlling the rate of increasing/decreasing the two cables' forces makes it possible to generate different release directions.

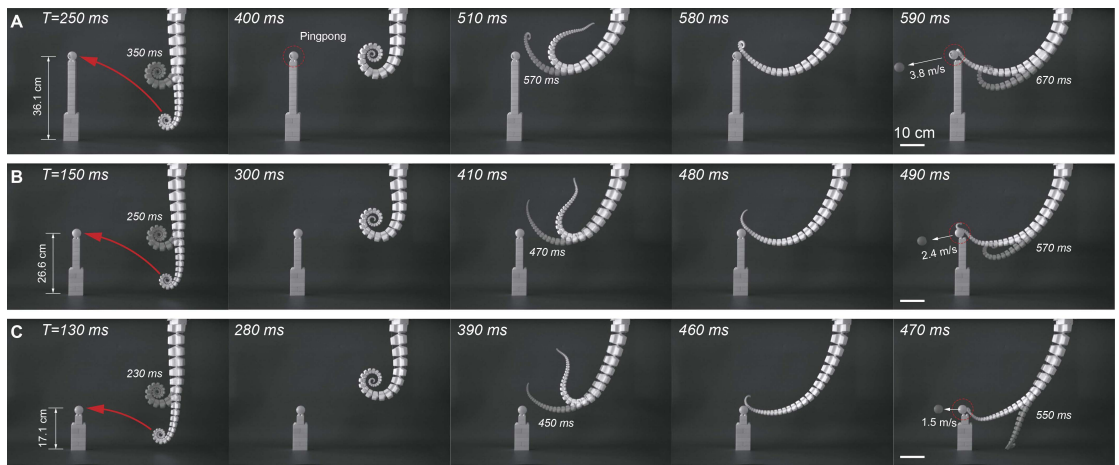


Figure S13. Whipping. (A)-(C) The robot first curls up when pulling two cables, and the accumulated elastic potential energy is released to produce a whipping action to pounce a pingpong ball (positioned at variable height).

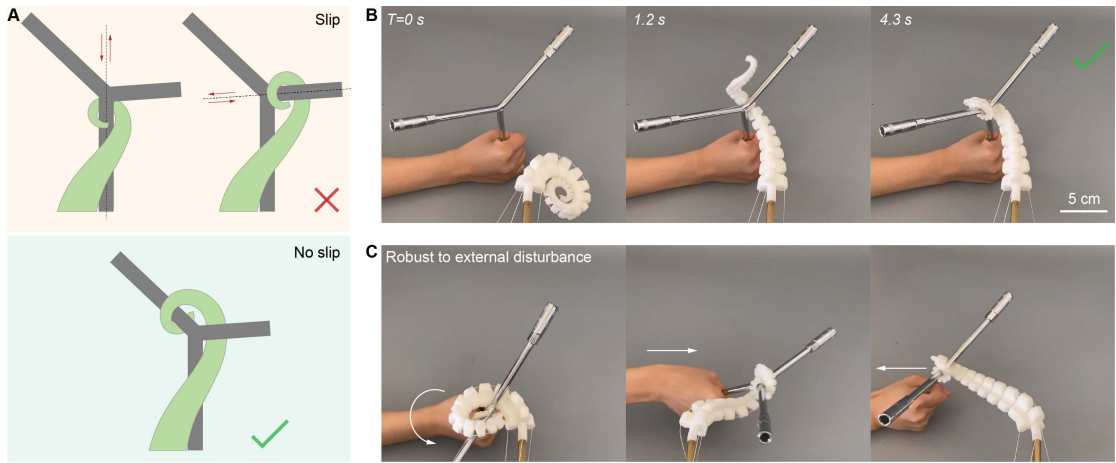


Figure S14. Non-slipable grasping. **(A)** Illustration of a non-slipable grasping strategy for the case of a tree-fork-shaped object. **(B)** Image sequence of a 3-cable SpiRob implementing the strategy to grasp a hexagonal wrench. **(C)** Images showing the robustness of the grip under external forces.

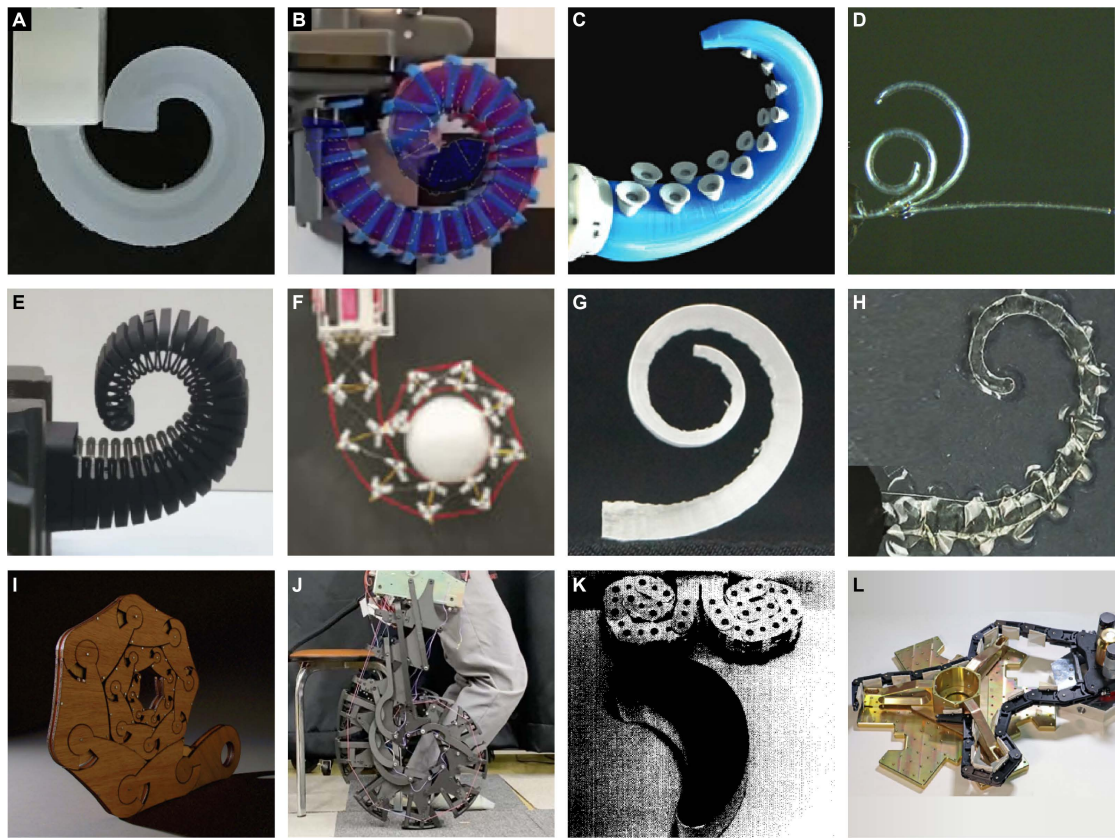


Figure S15. Spiral-shaped designs in the literature. (A)-(D) Pneumatically-actuated manipulators: the first two were cast by spiral-shaped molds^[S3,S4], while the latter produce a spiral bending when pressurized^[S5,S6]. (E) and (F) Cable-driven manipulators^[S7,S8]. (G) thermally-driven tendril-like gripper^[S9]. (H) Curling HASEL manipulator^[S10]. (I)-(L) Spiral-shaped designs with rigid links: The first two reproduce the spiral-shaped curling motion^[S11,S12], and the last two show the manipulators wrapping objects by uncurling on their surface^[S13,S14].

Supplemental References

- [S1]. Jiang, H., Wang, Z., Jin, Y., Chen, X., Li, P., Gan, Y., Lin, S., and Chen, X. (2021). Hierarchical control of soft manipulators towards unstructured interactions. *Int. J. Robot. Res.* *40*, 411–434. <https://doi.org/10.1177/0278364920979367>.
- [S2]. Coevoet, E., Escande, A., and Duriez, C. (2017). Optimization-Based Inverse Model of Soft Robots With Contact Handling. *IEEE Robot. Autom. Lett.* *2*, 1413–1419. <https://doi.org/10.1109/LRA.2017.2669367>.
- [S3]. Zhang, Z., Wang, X., Meng, D., and Liang, B. (2021). Bioinspired Spiral Soft Pneumatic Actuator and Its Characterization. *J. Bionic Eng.* *18*, 1101–1116. <https://doi.org/10.1007/s42235-021-00075-y>.
- [S4]. Zournatzis, I., Kalaitzakis, S., and Polygerinos, P. (2023). SoftER: A Spiral Soft Robotic Ejector for Sorting Applications. *IEEE Robot. Autom. Lett.* *8*, 7098–7105. <https://doi.org/10.1109/LRA.2023.3315206>.
- [S5]. Xie, Z., Domel, A.G., An, N., Green, C., Gong, Z., Wang, T., Knubben, E.M., Weaver, J.C., Bertoldi, K., and Wen, L. (2020). Octopus Arm-Inspired Tapered Soft Actuators with Suckers for Improved Grasping. *Soft Robot.* *7*, 639–648. <https://doi.org/10.1089/soro.2019.0082>.
- [S6]. Paek, J., Cho, I., and Kim, J. (2015). Microrobotic tentacles with spiral bending capability based on shape-engineered elastomeric microtubes. *Sci. Rep.* *5*, 10768. <https://doi.org/10.1038/srep10768>.
- [S7]. Taylor, I.H., Bawa, M., and Rodriguez, A. (2023). A Tactile-enabled Hybrid Rigid-Soft Continuum Manipulator for Forceful Enveloping Grasps via Scale Invariant Design. In *IEEE International Conference on Robotics and Automation (ICRA)*, pp. 10331–10337. <https://doi.org/10.1109/ICRA48891.2023.10161121>.
- [S8]. Zhang, J., Hu, Y., Li, Y., Ma, K., Wei, Y., Yang, J., Wu, Z., Rajabi, H., Peng, H., and Wu, J. (2022). Versatile Like a Seahorse Tail: A Bio - Inspired Programmable Continuum Robot For Conformal Grasping. *Adv. Intell. Syst.*, 2200263. <https://doi.org/10.1002/aisy.202200263>.
- [S9]. Wang, W., Li, C., Cho, M., and Ahn, S.-H. (2018). Soft Tendril-Inspired Grippers: Shape Morphing of Programmable Polymer–Paper Bilayer Composites. *ACS Appl. Mater. Interfaces* *10*, 10419–10427. <https://doi.org/10.1021/acsami.7b18079>.
- [S10]. Mitchell, S.K., Wang, X., Acome, E., Martin, T., Ly, K., Kellaris, N., Venkata, V.G., and Keplinger, C. (2019). An Easy-to-Implement Toolkit to Create Versatile and High-Performance HASEL Actuators for Untethered Soft Robots. *Adv. Sci.* *6*, 1900178. <https://doi.org/10.1002/advs.201900178>.
- [S11]. Henrich, A. (2021). John Edmark: Art in Motion. *Math. Mag.* *94*, 65–68. <https://doi.org/10.1080/0025570X.2021.1843890>.
- [S12]. Sugiura, S., Unde, J., Zhu, Y., and Hasegawa, Y. (2023). High-strength and flexible mechanism for body weight support. *ROBOMECH J.* *10*, 16. <https://doi.org/10.1186/s40648-023-00255-x>.
- [S13]. Hirose, S., and Umetani, Y. (1978). The development of soft gripper for the versatile robot hand. *Mech. Mach. Theory* *13*, 351–359. [https://doi.org/10.1016/0094-114X\(78\)90059-9](https://doi.org/10.1016/0094-114X(78)90059-9).
- [S14]. Glick, P.E., Van Crey, N., Tolley, M.T., and Ruffatto, D. (2020). Robust capture of unknown objects with a highly under-actuated gripper. In *IEEE International Conference on Robotics and Automation (ICRA)*, pp. 3996–4002. <https://doi.org/10.1109/ICRA40945.2020.9197100>.